GENETIC ABLATION OF CIAP2 PROTECTS AGAINST DENERVATION-INDUCED SKELETAL MUSCLE ATROPHY

Kristen Timusk

Thesis submitted to the
Faculty of Graduate and Postdoctoral Studies
In partial fulfillment of the requirements
For the MSc degree in Cellular and Molecular Medicine

Department of Cellular and Molecular Medicine
Faculty of Medicine
University of Ottawa

ABSTRACT

Skeletal muscle atrophy occurs as a secondary result from a number of conditions such as cancer cachexia, prolonged bed rest, and AIDS. Unfortunately, the cellular and molecular mechanisms behind atrophy are still poorly understood. It was recently found that the cellular inhibitors of apoptosis (cIAP1 and cIAP2) proteins play vital, yet redundant roles in the regulation of the NF-κB pathway, which is one of the most significant signalling pathways correlated with the loss of skeletal muscle mass in a number of conditions. I asked whether cIAP2 plays a role in skeletal muscle atrophy, using a denervation model which results in a consistent and rapid loss of muscle mass over a matter of days. cIAP2$^{-/-}$ and wild-type mice were denervated by removing a small portion of the sciatic nerve in the mid-thigh region of one limb, while the opposite limb was used as control. Fourteen days following sciatic nerve denervation, muscle tissue was harvested and the fibre cross-sectional area measured. I demonstrate that in the cIAP2$^{-/-}$ mice, muscle fibre size was spared when compared with their wild-type counterparts. To further support this phenotype, western blot analyses were performed with the muscles collected, which indicated a reduction in various muscle atrophy markers in the cIAP2$^{-/-}$ mice compared to wild-type, further supporting the observed protective phenotype. These data suggest that cIAP2 is a key regulator of skeletal muscle atrophy.

ACKNOWLEDGMENTS

First and foremost, I would like to thank my supervisor, Dr. Robert Korneluk, for taking me under his wing when his better judgement may have told him otherwise. Although my heart lies in medicine, you succeeded at instilling a passion for research in me, and I hope this became evident throughout my two years in the lab. Your enthusiasm and determination to better lives through science is truly inspirational.

Many thanks to all members of the Korneluk lab; I've shared laughs with each and every one of you, and as many of you know, laughter is a very important aspect of research in my books. In particular, special thanks to Nathalie Earl for all of your support during these two years and tremendous assistance in my work. Additionally, to Emeka Enwere – you deserve an award for enduring my endless questions. Your help and guidance are what have led me to this point, so I thank you immensely for that.

Thanks go to my committee members, Drs. Nadine Wiper-Bergeron, Bernard Jasmin and Lynn Megeney, for all of your help, support and advice.

Most importantly, I would like to sincerely thank my parents, Barbara and Evald Timusk; my brother, Evan Timusk; my sister-in-law, Teryn Bruni; and the love of my life, Nick Huffington. I certainly could not have done this without your endless support, motivation and love.

TABLE OF CONTENTS

Abstract ii
Acknowledements iii
Table of Contents iv
List of Figures vii
List of Tables ix
List of Abbreviations x
Chapter 1: Introduction 1
1.1 General Background on Skeletal Muscle 1
1.2 Skeletal Muscle Atrophy 1
1.3 Disuse Atrophy 5
1.4 Denervation-Induced Skeletal Muscle Atrophy 8
1.5 Apoptosis and Skeletal Muscle Atrophy 9
1.6 NF-κB Involvement in Skeletal Muscle Atrophy 14
1.7 TNF-like Weak Inducer of Apoptosis 19
1.8 Objectives 21
Chapter 2: Materials and Methods 22
2.1 Animal Models 22
2.1.1 C57BL/6 Mice 22
2.1.2 cIAP2$^{-/-}$ Mice 22
2.2 Protein and RNA Sources and Extraction 23
2.2.1 Denervation 23
2.2.2 Protein Extraction 23
2.2.3 RNA Extraction 24
2.3 Fibre cross-sectional analysis 24
2.3.1 Tissue sectioning 24
2.3.2 Haemotoxylin and Eosin staining 25
2.3.3 Measurement of Fibre Cross-Sectional Area 25
2.3.4 Data Analysis 25
2.4 Immunohistochemical Analysis of Fibre Type Composition 26

2.4.1 Immunofluorescent Staining 26
2.4.2 Fibre Type Composition Analysis 27
2.4.3 Data Analysis 27
2.5 Protein Level Analysis of TNF-like Weak Inducer of Apoptosis 27
2.5.1 ELISA Assay 27
2.5.2 Data Analysis 28
2.6 Polymerase Chain Reaction and Protein Analysis of Marker of Atrophy Genes 28
2.6.1 Quantitative Real-Time Reverse Transcriptase Polymerase Chain Reaction 28
2.6.2 Western Blot Analysis 29
2.6 Effects of TWEAK on Primary Myotubes 29
2.6.1 Cell Culture 29
Chapter 3: Results 32
3.1 In Vivo Analysis of the Effects of the Loss of cIAP2 on Skeletal Muscle Atrophy 32
3.1.1 Denervation-Induced Skeletal Muscle Atrophy is Rescued by the Loss of cIAP2 7 Days Post-Denervation 32
3.1.2 Protection Against Denervation-Induced Skeletal Muscle Atrophy is Maintained 14 Days Post-Denervation 43
3.1.3 Fibre Size Maintenance is Diminished 28 Days after Denervation in the Absence of cIAP2 54
3.1.4 Analysis of Various Markers of Atrophy and IAP Expression by Western Blot Analysis 57
3.1.5 Absence of cIAP2 Protects Soleus Muscle Fibres from Shifting to a Fast Phenotype 14 days After Denervation 62
3.1.6 Verification of Protective Phenotype in cIAP2$^{-/-}$ Mice Compared to Wild-Type and Heterozygous Littermates 65
3.1.7 Fn14 is not Induced in Response to Denervation 67
3.1.8 TWEAK Serum Levels are Unaltered in cIAP2$^{-/-}$ Mice 69
3.2 In Vitro Characterization of the Effects of TWEAK on cIAP2$^{-/-}$ Myotubes 71
3.2.1 cIAP2$^{-/-}$ Myotubes Atrophy in Response to Treatment with Soluble TWEAK 71
Chapter 4: Discussion 75

4.1 Effects of the Loss of cIAP2 on Skeletal Muscle Atrophy 75
4.1.1 Genetic Ablation of cIAP2 Spares Skeletal Muscle Fibre CSA in Response to Denervation 75
4.1.2 Absence of cIAP2 Protects SOL and Fibres from Undergoing the Fibre-Type Switch Characteristic of Atrophy 77
4.1.3 Markers of Atrophy are not Induced in Denervated cIAP2$^{-/-}$ Muscle 79
4.1.4 Involvement of the TWEAK/Fn14 System in the Protection Against Atrophy in the Absence of cIAP2 80
4.1.5 Conclusions and Future Directions 82
References 84

LIST OF FIGURES

Figure 1: Flow diagram demonstrating the disuse atrophy cascade that leads to muscle proteolysis.....6

Figure 2: Domain structure of cIAP1 and cIAP2.....12

Figure 3: Absence of cIAP2 protects TA fibre cross-sectional area from denervation-induced atrophy 7 days post-denervation.....34

Figure 4: Fibre cross-sectional area fails to undergo a dramatic shift toward smaller fibres 7 days following denervation in cIAP2$^{-/-}$ TA compared to C57BL/6.....35

Figure 5: Fibre cross-sectional area is spared 7 days following denervation in cIAP2$^{-/-}$ TA compared to C57BL/6.....36

Figure 6: Absence of cIAP2 protects SOL fibre cross-sectional area from denervation-induced atrophy 7 days post-denervation.....38

Figure 7: Fibre cross-sectional area fails to undergo a dramatic shift toward smaller fibres 7 days following denervation in cIAP2$^{-/-}$ SOL compared to C57BL/6.....39

Figure 8: Fibre cross-sectional area is spared 7 days following denervation in cIAP2$^{-/-}$ SOL compared to C57BL/6.....40

Figure 9: Absence of cIAP2 protects EDL fibre cross-sectional area from denervation-induced atrophy 7 days post-denervation.....41

Figure 10: Fibre cross-sectional area fails to undergo a dramatic shift toward smaller fibres 7 days following denervation in cIAP2$^{-/-}$ EDL compared to C57BL/6.....42

Figure 11: Fibre cross-sectional area is spared 7 days following denervation in cIAP2$^{-/-}$ EDL compared to C57BL/6.....43

Figure 12: Absence of cIAP2 protects TA fibre cross-sectional area from denervation-induced atrophy 14 days post-denervation.....45

Figure 13: Fibre cross-sectional area fails to undergo a dramatic shift toward smaller fibres 14 days following denervation in cIAP2$^{-/-}$ TA compared to C57BL/6.....46

Figure 14: Fibre cross-sectional area is spared 14 days following denervation in cIAP2$^{-/-}$ TA compared to C57BL/6.....47

Figure 15: Absence of cIAP2 protects SOL fibre cross-sectional area from denervation-induced atrophy 14 days post-denervation.....48

Figure 16: Fibre cross-sectional area fails to undergo a dramatic shift toward smaller fibres 14 days following denervation in cIAP2$^{-/-}$ SOL compared to C57BL/6.....49

Figure 17: Fibre cross-sectional area is spared 14 days following denervation in cIAP2$^{-/-}$ SOL compared to C57BL/6.....50

Figure 18: Absence of cIAP2 protects EDL fibre cross-sectional area from denervation-induced atrophy 14 days post-denervation.....51

Figure 19: Fibre cross-sectional area fails to undergo a dramatic shift toward smaller fibres 14 days following denervation in cIAP2$^{-/-}$ EDL compared to C57BL/6.....52

Figure 20: Fibre cross-sectional area is spared 14 days following denervation in cIAP2$^{-/-}$ EDL compared to C57BL/6.....54

Figure 21: Fibre cross-sectional area fails to undergo a dramatic shift toward smaller fibres 28 days following denervation in cIAP2$^{-/-}$ TA compared to C57BL/6.....56

Figure 22: Fibre cross-sectional area is spared 28 days following denervation in cIAP2$^{-/-}$ TA compared to C57BL/6.....57

Figure 23: Representative western blots of GAS muscle 7 days following denervation.....61

Figure 24: Representative western blots of GAS muscle 14 days following denervation.....62

Figure 25: Loss of cIAP2 results in the failure of soleus muscle to undergo the characteristic increase in fast-twitch fibres following denervation.....64

Figure 26: Type I fibres are spared in cIAP2$^{-/-}$ SOL 14 days after denervation.....65

Figure 27: Fibre cross-sectional area is spared 14 days following denervation in cIAP2$^{-/-}$ TA compared to WT and HET littermates.....67

Figure 28: Fn14 induction is inhibited in cIAP2$^{-/-}$ gastrocnemius muscle 7 days following denervation.....69

Figure 29: TWEAK serum levels show no significant difference cIAP2$^{-/-}$ compared to C57BL/6.....71

Figure 30: cIAP2$^{-/-}$ primary myotubes respond to TWEAK in a similar fashion as wild-type myotubes.....74-75

LIST OF TABLES

Table 1: Primary Antibodies Used in Experiments.....32

LIST OF ABBREVIATIONS

BIR	Baculoviral IAP Repeat
cIAP1/2	Cellular Inhibitor of Apoptosis-1/2
COPD	Chronic Obstructive Pulmonary Disease
CSA	Cross-Sectional Area
CTRL	Control
DEN	Denervated
DMD	Duchenne Muscular Dystrophy
DMEM	Dulbecco's Modified Eagle Medium
DMSO	Dimethyl Sulfoxide
EDL	Extensor Digitorum Longus
ELISA	Enzyme-linked Immunosorbant Assay
FBS	Fetal Bovine Serum
FGF	Fibroblast Growth Factor
Fn14	Fibroblast Growth Factor-Inducible 14
GAPDH	Glyceraldehyde Phosphate Dehydrogenase
GAS	Gastrocnemius
HGF	Hepatocyte Growth Factor
H&E	Haemotoxylin and Eosin
IAP	Inhibitor of Apoptosis
IκB	Inhibitor of Kappa B
IKK	Inhibitor of Kappa B Kinase
MAFbx	Muscle Atrophy F-Box
MHC	Myosin Heavy Chain
MuRF1	Muscle-specific Ring Finger protein 1
NF-κB	Nuclear Factor-κB
OCT	Optimal Cutting Temperature
OD	Optical Density
PBS	Phosphate-Buffered Saline
PCD	Programmed Cell Death
RING	Really Interested New Gene
SEM	Standard Error of the Mean
SMC	Smac Mimetic Compound
RHD	Rel Homology Domain
RIP1	Receptor Interacting Protein
TA	Tibialis Anterior
TNFα	Tumour Necrosis Factor-α
TRADD	TNFR-Associated Death Domain
TRAF	TNFR-Associated Factor
TWEAK	Tumour Necrosis Factor-like Weak Inducer of Apoptosis
WT	Wild-Type
XIAP	X-linked Inhibitor of Apoptosis

1. Introduction

1.1 General Background on Skeletal Muscle

Skeletal (striated) muscle is the most abundant muscle and largest organ in the human body and is responsible for a number of necessary functions, including locomotor activity, postural behaviour and breathing to name a few (Charge and Rudnicki, 2004). Given its extreme importance as a requirement for living, the maintenance of this tissue is essential. Under normal conditions, muscle tissue maintains its mass and function as a result of a balance between protein synthesis and protein degradation related to anabolic and catabolic processes, correspondingly (Saini et al., 2009). However, as an outcome of a number of conditions, the levels of protein degradation sometimes exceed those of protein synthesis, causing the muscle to waste rather than maintain its size and function, thus resulting in skeletal muscle atrophy (Saini et al., 2009).

1.2 Skeletal Muscle Atrophy

Most often occurring as a secondary result, atrophy can be induced by several disease states including cancer (cachexia), sepsis and muscular dystrophies, but also as a result of conditions including fasting, immobilization, aging and denervation (Saini et al., 2009; Cohen et al., 2009; Lecker et al., 1999, 2006; Jackman and Kandarian, 2004). Atrophy is characterized by the reduction in size of the muscle fibre cross-sectional area and fibre diameter, muscle proteolysis, fibre type switch, and loss of strength and muscle mass leading to increased fatigue and insulin resistance (Li et al., 2008; Jackman and Kandarian, 2004; Kandarian and Jackman, 2006; Ferreira et al., 2008; Appell 1990).

Unfortunately, muscle wasting often contributes significantly to patient mortality in numerous disease states and there are currently no effective treatments, thus making the importance of research in this field and gaining a better understanding of atrophy quite evident.

The molecular triggers and signalling pathways leading to skeletal muscle atrophy vary depending on the root cause or condition of the atrophy. Though it has been well defined that following muscle disuse, the rate of protein synthesis is severely decreased and that of protein degradation is increased therefore leading to atrophy (Goldspink et al., 1986; Loughna et al., 1986; Thomason and Booth, 1989), the upstream signals initiating these effects are still unclear.

Normally, muscle maintenance occurs as a result of an equilibrium between protein synthesis and degradation related to equivalent rates of anabolic and catabolic processes, respectively. When protein synthesis exceeds that of protein degradation, the outcome is muscle hypertrophy, or growth. Opposing this process, muscles decrease in size (atrophy) when protein degradation prevails over protein synthesis. Muscle atrophy resulting from various disease states is often initiated by a number of inflammatory cytokines, whereas the initiating culprits of disuse atrophy include a decrease in muscle tension and contractile activity. However, although the triggers causing atrophy may vary, the outcome of a decrease in muscle mass due to the stimulation of muscle proteolysis remains the same regardless of the initiator.

There are four known pathways which lead to the process of muscle breakdown, and these are the ubiquitin-proteasome pathway (Attaix et al., 2005; Cao et al., 2005); Tisdale, 2005), the lysosomal pathway (Farges et al., 2002; Busquets et al., 2006) the

calpain-calpastatin pathway (Bartoli and Richard, 2005; Costelli et al., 2005; Hasselgreen et al., 2005) and the apoptosis or programmed cell death pathway (Lee et al., 2004; Leeuwenburgh et al., 2005; Siu and Alway, 2006). Activation of one or more of these pathways can explain the muscle wasting that occurs in multiple forms of atrophy, however, not all pathways are necessarily activated in each condition (Lynch et al., 2007). Muscle is similar to all other tissues in that the majority of intracellular proteolysis that occurs does so through the ubiquitin-proteasome pathway (Rock et al., 1994). Furthermore, it has become well-established that this system is of great importance with regard to the proteolysis that occurs in muscle as it atrophies (Cao et al., 2005; Lecker, Solomon, Mitch et al., 1999; Lecker, Solomon, Price et al., 1999). The ubiquitin-proteasome pathway is primarily defined by the action of enzymes which link the polypeptide cofactor ubiquitin to protein substrates to target them for degradation (Glickman and Ciechanover, 2002). There are three distinct components required for the addition of ubiquitin chains to a protein substrate: an E1 ubiquitin-activating enzyme and an E2 ubiquitin-conjugating enzyme, which both function in preparing ubiquitin for conjugation, as well as an E3 ubiquitin-ligating enzyme (Hershko and Ciechanover, 1998). These enzymes work together to carry out this process and although all three components are necessary, the most important is perhaps the E3 ubiquitin-ligating enzyme as it is responsible for determining which proteins are to be degraded by the proteasome and for pairing the activated ubiquitin with the protein substrates. The two general categories that E3s can be separated into are based on whether they contain either "homologous to E6-AP carboxyterminus" (HECT) domains, or "Really Interesting New Gene" (RING) fingers (Cao et al., 2005; Jackson et al., 2000). HECT-domain E3s are

fairly similar to E2s in that they directly bind to activated ubiquitin, thus functioning as a part of the enzymatic conjugation cascade (Scheffner et al., 1995) whereas RING-containing E3s function by catalyzing ubiquitin conjugation in a less direct fashion (Lorick et al., 1999; Seol et al., 1999).

Interestingly, the majority of E3s contain RING finger domains that are generally located in a small protein subunit of a much larger complex which displays ubiquitin ligase activity. Among the E3s of relevance to the process of muscle atrophy is a gene encoding the Muscle-specific Ring Finger protein 1 (MuRF1) (Bodine et al., 2001). MuRF1 is a 40 kDa protein containing a RING domain at its amino-terminal end and two coiled-coil domains in the central region (Centner et al., 2001; Spencer et al., 2000). MuRF1 has been established to be upregulated in atrophying muscle, consistent with an essential role in both the development and progression of atrophy (Jones et al., 2004; Lecker et al., 2004) and thus it is used as one of two definitive markers of muscle wasting. Similar to MuRF1, muscle atrophy F-box (MAFbx) or Atrogin-1 is the second muscle-specific E3 ubiquitin ligase that is also induced in atrophying muscle (Gomes et al., 2001). The MAFbx/Atrogin-1 gene contains a characteristic F-box domain which places it in the class of E3s known as Skp1-Cullen-Fbox, or SCF complexes (Gomes et al., 2001), and it is this F-box domain that is responsible for linking the other components of the E3 complex to the protein targeted for degradation. Notably, both MuRF1 and MAFbx/Atrogin-1 expression have been found to increase in the early initiation stages of muscle wasting, therefore making them prime candidates as early markers of atrophy.

Although there has been much interest in atrophy within the past several years, the cellular and molecular mechanisms behind the process of muscle wasting, specifically disuse atrophy, are still poorly understood.

1.3 Disuse Atrophy

As stated previously, there are various causes of skeletal muscle atrophy which can be categorized into two broad areas, namely disease states and disuse conditions. Although the molecular targets are similar between the different forms, the triggers initiating muscle wasting vary greatly. Disuse models of atrophy involve inducing the state of atrophy by physical means such as hind-limb suspension, bed-rest, spaceflight or denervation. Following the initial physiological stimulus wherein the muscle no longer weight-bears nor contracts with tension, various molecules and pathways implicated in disuse atrophy carry out muscle proteolysis (Fig. 1). The significant atrophy that occurs as a result of muscle disuse is coupled with alterations in contractile properties and myosin heavy chain expression, along with a shift toward a predominantly glycolytic pattern of metabolism (Sacheck et al., 2007; Roy et al., 2000; Roy et al., 2002; Huey et al., 2001). Though it has become well established that in response to muscle disuse, the rate of protein synthesis decreases while that of protein degradation increases (Goldspink et al., 1986; Loughna et al., 1986; Thomason and Booth, 1989), the upstream molecules regulating these modifications are still not well understood.

While the molecular basis of disuse muscle atrophy is not yet well defined, there are a number of potential triggers and pathways that have been identified to play a role

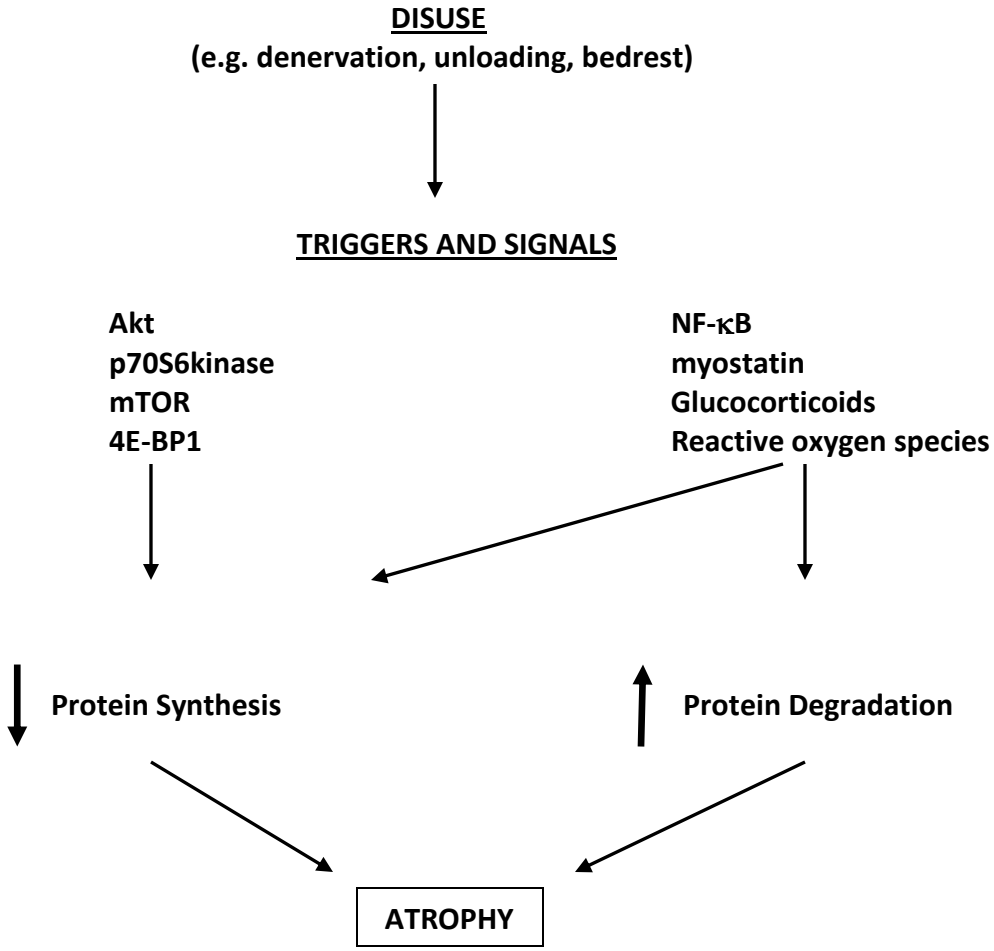

Figure 1. Flow diagram demonstrating the disuse atrophy cascade that leads to muscle proteolysis.

Upon muscle unloading, various triggers and signals are activated which in turn lead to a decrease in protein synthesis and an increase in protein degradation. This imbalance in protein maintenance leads to skeletal muscle atrophy. (Adapted from Jackman and Kandarian, 2004)

in the regulation of disuse atrophy. The protein degradation that occurs as a result of muscle disuse has been linked to the activation of three particular proteolytic pathways, specifically those involving the Ca^{2+} -dependent calpains (Tidball and Spencer, 2002), the lysosomal cathepsins (Taillandier et al., 1996) and the ubiquitin-proteasome system (review by Reid, 2005) (Lynch et al., 2007). However, data demonstrating the potential role of calpains and calpastatin in disuse atrophy (Taillandier et al., 1996; Tidball and Spencer, 2002) have been quite ambiguous, therefore signifying the necessity of further work in order to gain a better understanding of the involvement of these pathways throughout muscle disuse (Lynch et al., 2007). Common to all forms of atrophy, gene expression analysis has identified a rapid increase in expression of both MuRF1 and MAFbx/Atrogin-1 E3 ligases during the first few days of disuse atrophy, supporting the important role of the ubiquitin-proteasome pathway in the process of muscle proteolysis. Conversely, mRNA encoding for cathepsins C, D and L has been found to be induced following 7-14 days of muscle disuse (Stevenson et al., 2003), thus suggesting that lysosomal proteases come into play only after long-standing periods of disuse.

On a physiological level, disuse atrophy has been found to affect fast- and slow-twitch skeletal muscle fibres differently. Muscles composed predominantly of slow-twitch (type I) fibres, as in the soleus, are affected by atrophy to a greater extent (Thomason and Booth, 1990) than muscles composed primarily of fast-twitch (type II) fibres (Bigard et al., 1998) such as the tibialis anterior (TA). Also of interest, normal weight bearing muscles (those consisting mostly of type I fibres) tend to shift toward a fast-twitch phenotype upon muscle unloading while adopting a faster velocity of shortening as well as a faster rate of relaxation (Lynch et al., 2007; Bigard et al., 1998;

Stevenson et al., 2003). Although the mechanisms accountable for these phenotypic changes are currently not known, it is thought to be likely due to both neuronal and myogenic factors (Lynch et al., 2007). Interestingly, although this change occurs in muscle fibre composition as a result of disuse atrophy, muscle fatigability remains unaffected, which could be explained by the fact that there appears to be no change in the oxidative capacity of the muscle (Lynch et al., 2007; Bigard et al, 1998; Stein and Wade, 2005).

1.4 Denervation-Induced Skeletal Muscle Atrophy

The nervous system is proposed to affect peripheral muscle properties in two ways, either through the propagation of motor impulses and/or through the release of chemical factors which perform in parallel to muscle activation (Midrio, 2006). When this neuromuscular signalling is impaired, the end result is muscle atrophy and in some cases paralysis, as proper nerve function is imperative for muscle function. The reduction of neuromuscular function occurs in a number of disuse conditions including unloading, immobilization and denervation (Jackman and Kandarian, 2008). Denervation can be described as the loss of nerve supply resulting from motor neuron or chemical death, or as an outcome of physical injury (Foletta et al., 2011). This model is commonly used to study disuse atrophy, as the loss of neural innervation to skeletal muscle results in a number of changes on a biochemical, morphological and functional level which leads to a rapid and consistent decrease in muscle protein content, as well as a reduction in muscle fibre size. Thus denervation is a reliable and efficient model of disuse atrophy.

Research has shown that denervation stimulates the degradation of muscle proteins, most notably contractile protein through the activation of the ubiquitin-proteasome pathway in addition to the induction of various specific proteases (Furuno et al., 1990; Goldberg, 1969; Goldberg and Goodman, 1969; Goldspink, 1976). Similar to other forms of disuse atrophy, Guttman reported in 1948 that all muscles were not affected equally. For example, the rate of atrophy was more rapid in the soleus (primarily slow-twitch) than in the EDL (primarily fast-twitch). In addition, it has since been shown by Patterson et al. (2006) that denervation results in a substantial shift in muscle phenotype from slow-twitch fibres to a more intermediate phenotype comprised of hybrid fast-slow fibres (Lynch et al., 2007).

Irrespective of the primary factor leading to the denervation of skeletal muscle, the result of a decrease in muscle mass as well as altered contractile properties remains the same and is due to the activation of various signalling pathways, including apoptosis. Interestingly enough, denervation is one of the only forms of atrophy in which apoptosis plays a considerable role in the origin of muscle wasting and loss of function. (Lynch et al., 2007)

1.5 Apoptosis and Skeletal Muscle Atrophy

Apoptosis is a highly regulated process involving the programmed deletion of cells in response to a number of intrinsic and extrinsic stimuli (Fadeel and Orrenius, 2005). Also referred to as programmed cell death (PCD), the autodestruction of cells regulated by apoptosis is crucial for the development and maintenance of tissue homeostasis in multicellular organisms (Leist and Jaattela, 2001; Hu and Yang, 2003).

Failure of cells to undergo apoptosis, or rather, inappropriate cell death is the basis of numerous disease pathologies (LaCasse et al., 2008).

Apoptosis was first distinguished from necrotic cell death in 1972 by Kerr and colleagues. Apoptosis differs from necrosis in that necrosis is an accidental or pathological form of cell death, whereas apoptosis is a well-orchestrated and highly regulated pathway leading to the destruction of cells. Whether a cell undergoes necrosis or apoptosis is to some extent a reflection of the magnitude of the insult (Fadeel and Orrenius, 2005; Bonfoco et al., 1995; Ankarcrona et al., 1995). There are numerous biochemical indicators of apoptosis that have been elucidated, including nuclear DNA fragmentation, chromatin condensation, and activation of caspases. The majority of morphological changes observed during apoptosis are found to be primarily caused by the activation of a set of cysteine aspartate specific proteases (caspases) in apoptotic cells (Fadeel and Orrenius, 2005), thus the apoptotic pathway is often considered a caspase-mediated mode of cell death.

There have been over a dozen mammalian caspases identified to date, and at least eight of these play significant roles in the process of apoptosis (Shi, 2002). These eight caspases involved in apoptosis can be placed into; the initiator caspases (-2, -8, -9 and -10), characterized by their extended N-terminal prodomain imperative for their function, and the effector caspases (-3, -6, and 7) whose prodomain sequences contain 20-30 residues (Shi, 2002). All caspases are inactive zymogens when first synthesized in cells; but during apoptosis they undergo proteolytic activation and are converted into mature enzymes (Alenzi et al., 2010). Autoactivated initiator caspases are responsible for the activation of effector caspases, through cleavage at precise internal Asp residues which

divide the small and large subunits (Shi, 2002). Upon activation, the effector caspases regulate the proteolytic cleavage of various cellular targets including regulatory proteins, structural components (actin and nuclear laminin), inhibitors of deoxyribonuclease as well as a number of other proapoptotic proteins and caspases (Shi, 2002).

Due to the fact that caspases ultimately drive apoptosis, it is crucial that these proteases are very tightly regulated in order to prevent inappropriate cell death from occurring. This regulation of caspase activity transpires as a result of the inhibition of active proteases by various members of the Bcl-2 family as well as the Inhibitor of Apoptosis Proteins (IAPs). Within mammals, the best recognized mechanism for control of caspase activation is driven by the members of the IAP family and their direct interaction with this proteolytic pathway (Eckelman and Salvesen, 2006). The IAPs encompass a group of highly conserved proteins vital in the regulation of apoptosis (Hu and Yang, 2003; Deveraux and Reed, 1999). The IAP gene family functions in regulating the life and death decisions of the cell in response to a number of daily stressors and are the only known endogenous proteins that control the activity of both initiator and effector caspases. Of particular interest within this family of IAPs are the cellular IAPs 1 and 2 (cIAP1 and cIAP2), characterized by their three baculovirus IAP repeat (BIR) domains which aid in their binding to caspases among other proteins (Fig. 2) (Eckelman and Salvesen, 2006). BIR motifs are zinc-binding folds of roughly 70 amino acid residues (Birnbaum et al., 1994; Hinds et al., 1999; Sun et al., 1999) that are essential for the anti-

Figure 2.

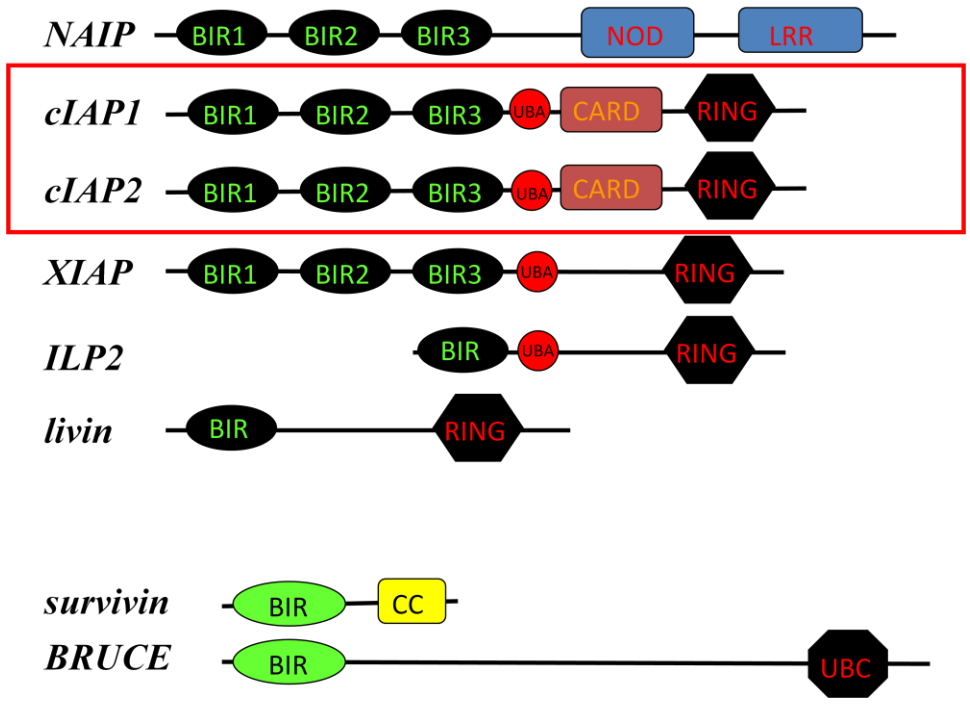

Figure 2. Domain structure of cIAP1 and cIAP2.

The domain organization of all eight human IAPs is shown, with the focus on cIAP1 and cIAP2. Both cIAP1 and cIAP2 are characterized by their three BIR domains. They also each contain a CARD domain located in the linker region between the BIR domains and the RING zinc finger domain, located at the carboxy terminus.

apoptotic properties of the IAPs (Gyrd-Hansen and Meier, 2010). Both cIAP1 and cIAP2 contain a unique caspase recruitment domain (CARD) of unknown function, thought to play a role in protein-protein interactions (Martin, 2001).

While the presence of IAPs in cells is required to avoid unnecessary apoptosis, their constant expression can lead to a suppression of appropriate cell death, leading to a number of problems. This issue is successfully controlled by the endogenous presence of IAP antagonists, in particular, Smac/DIABLO (second mitochondria-derived activator of caspases, direct IAP-binding protein with low PI), which is a pro-apoptotic mitochondrial protein. The characteristic N-terminal motif of IAP inhibitors is responsible for confining Smac to the mitochondria. Upon apoptotic stimuli, the N-terminal domain of Smac is proteolytically cleaved, an AVPI-containing amino terminus polypeptide is formed (Burri et al., 2005) and Smac is released into the cytoplasm. Due to the presence of the AVPI motif, Smac then has the ability to bind to IAPs and prevent IAP-mediated caspase inhibition, thus promoting apoptosis.

Smac is a member of a particular class of cellular IAP antagonists known as IBM (IAP binding motif) proteins. These inhibitors contain a characteristic N-terminal motif which aids in their binding to IAPs. Investigation of the properties of this N-terminal domain has led to the development of a class of synthetic cancer therapeutics, known as Smac mimetic compounds (SMCs) which can either bind IAPs in monovalent or bivalent fashion. The notable difference between these two forms is that the monovalent SMCs have a single AVPI binding motif and the bivalent compound contains two AVPI binding motifs joined through a linker (Sun *et al*., 2008). SMCs induce cell death through their binding to and inhibition of both cIAP1 and 2.

Research on the IAP family has been extensive and is continually moving forward. Although they were originally thought to be direct caspase inhibitors (Roy et al., 1997), data has more recently indicated that cIAP1 and cIAP2 bind to but do not directly inhibit caspases, thus leaving the true biologic role of these proteins in apoptosis to be unclear (Eckelman and Salvesen, 2006). Although their biologic role in entirety remains enigmatic, it is however well established that both cIAP1 and cIAP2 play crucial roles in the regulation of the NF-κB pathway; a pathway in which increasing evidence suggests serves as a key component in the loss of skeletal muscle mass, one of the hallmark features of atrophy (Li et al., 2008).

1.6 NF-κB Involvement in Skeletal Muscle Atrophy

Although little is known about the systemic and muscle-specific mediators of denervation-induced atrophy, it is however well-established that the NF-κB pathway is activated in denervated muscle tissue. Nuclear factor-kappa B (NF-κB) refers to an elaborately regulated cellular pathway responsible for the control of a number of biological processes, including innate and adaptive immunity, cell proliferation, and apoptosis (Mourkioti et al., 2006; Zarnegar et al., 2008; Bonizzi and Karin, 2004; Courtois and Gilmore, 2006.). In mammals, the NF-κB family consists of a set of five members: NF-κB1 (p105/p50), NF-κB2 (p100/p52), RelA (p65), RelB, and c-Rel (Bonizzi and Karin, 2004; Hayden and Ghosh, 2008). These family members are characterized by a highly conserved DNA-binding/dimerization domain in which they share, known as the Rel homology domain (RHD) (Gilmore, 1990). This RHD, within

itself, mediates the dimerization of Rel/NF-κB proteins through specific motifs (May and Ghosh, 1997; Li et al., 2008).

Under normal conditions, NF-κB heterodimers remain latent in the cytoplasm of most cells, bound by IκB proteins (Gilmore, 2006). However, activation of the NF-κB pathway occurs in response to various stimuli, including viral and bacterial infection, exposure to proinflammatory cytokines (e.g. TNFα), growth factors, mitogens, as well as to modulators of oxidative and biochemical stress (Li et al., 2008). Depending on the stimuli presented, a number of signal transduction pathways may be initiated, each of which involve distinct adaptor and signalling proteins. The majority of these signalling pathways congregate on the inhibitor of κB (IκB) kinase (IKK) complex that is made up of two catalytic subunits (IKK-α and IKK-β), and a regulatory subunit (IKK-y/NEMO) (Li et al., 2008). Depending on the subunits of the IKK complex involved in the signalling and in turn, the transcription factors involved, there are two pathways which can be activated; the classical and the alternative pathway (Li et al., 2008). Depending on which becomes activated, each pathway regulates their own specific sets of target genes (Li et al., 2008).

Pathological activation of NF-κB occurs in a number of muscle diseases, including Duchenne muscular dystrophy (DMD), inflammatory myopathies and muscle atrophy (Peterson and Guttridge, 2008; Monici et al., 2003; Li et al., 2008). As stated in Li et al. (2008), emerging evidence suggests that NF-κB is one of the most significant signalling pathways correlated with the loss of skeletal muscle mass in a number of physiological and pathophysiological conditions. Activation of the NF-κB pathway in skeletal muscle results in the degradation of certain muscle proteins, induced

inflammation and fibrosis, and impeded regeneration of myofibres during and after atrophy (Li et al., 2008).

The involvement of increased NF-κB activity in skeletal muscle atrophy can be broken down into three potential mechanisms. First, NF-κB can lead to the increased expression of a number of proteins involved in the ubiquitin-proteasome pathway, including MuRF1, that are responsible for the degradation of specific muscle proteins throughout atrophy. Second, NF-κB could potentially increase the expression of inflammation-associated molecules which promote muscle wasting. Third, NF-κB is also capable of disrupting the process of myogenic differentiation which is likely essential for the regeneration of skeletal muscle tissue post-atrophy (Li et al., 2008). Various studies have demonstrated that an increase in NF-κB activity is associated with several forms of skeletal muscle atrophy, including that associated with muscular dystrophy, cancer cachexia, sepsis, chronic obstructive pulmonary disease (COPD), diabetes, disuse and aging (Li et al., 2009). Hunter et al. (2002) established that, in response to hindlimb unloading, NF-κB DNA-binding and reporter gene activities were both increased in the soleus muscle of the rat. Specifically, nuclear levels of the NF-κB/IκB family proteins p50, c-Rel and Bcl3 were significantly increased when compared to weight-bearing rats (Li et al., 2009). Furthermore, the role of the NF-κB pathway specifically in denervation-induced atrophy has recently been further elucidated by Mourkioti et al. 2006. This study demonstrated that targeted deletion of IKK2 subunit of the IKK complex in mice leads to an increase in intermediate type fibres, and total cross-sectional area as well as to increases in specific twitch and titanic forces in the soleus muscle (Li et al., 2009). In addition, activation of NF-κB in response to sciatic nerve denervation in muscle-

restricted IKK2-deficent mice did not lead to loss of skeletal muscle mass and function, when compared to controls (Mourkioti et al., 2006).

A second transgenic approach in mice was taken by Cai et al. (2004) who also investigated the role of NF-κB in denervation-induced atrophy, by overexpressing a super-repressor mutant of the NF-κB inhibitory protein IκBα (IκBαSR) in skeletal muscle. They found that, compared to the 9-fold increase of NF-κB in wild-type mice at 14 days following denervation, there was only a 1.5-fold increase in NF-κB activity in the IκBαSR-expressing hindlimb muscles of the transgenic mice (Li et al., 2009). In addition, the typical atrophic features of loss of muscle mass and fibre size in response to denervation were dramatically blunted due to the IκBαSR overexpression (Cai et al., 2004). These results suggest that NF-κB activity does in fact play a key role in denervation-induced skeletal muscle atrophy.

With the advancement in our understanding of NF-κB signal transduction, several papers have established the important role of both cIAP1 and cIAP2 in the critical regulation of this pathway through the cytokine tumour necrosis factor-alpha (TNFα). TNFα is a pleiotropic cytokine implicated in a number of biologic functions, including tissue regeneration in response to injury, and in the proper development and functioning of the immune system (Wajant et al., 2003). TNFα is perhaps the most notable cytokine involved in the pathogenesis of muscle atrophy, and together with the aberrant activation of NF-κB, plays a significant role in this condition (Cai et al., 2004; Li et al., 2008).

In the majority of cells, TNFα signals via its receptor TNF-R1, resulting in the activation of the proinflammatory transcription factor NF-κB (Wajant et al., 2003). Through the binding of TNF-R1 to TNFα, recruitment of the adaptor protein TNFR-

associated death domain (TRADD) to the death domain of the receptor is induced. It is by means of this death domain and amino-terminal region that receptor-interacting protein (RIP1) and TNFR-associated factor 2 (TRAF2) are recruited, the latter of which cIAP1 and 2 are bound to (Varfolomeev et al., 2008).

Mahoney and colleagues (2008) have demonstrated that both cIAP1 and cIAP2 hold biologically relevant roles in facilitating TNFα-mediated NF-κB activation, however, complete knowledge of each protein's individual role is still unknown. Mahoney and coworkers suggest that perhaps cIAP1 acts primarily in the initial activation of NF-κB, whereas cIAP2 may instead participate in the "fine-tuning" of the NF-κB response. Also established by both Mahoney et al. (2008) and Varfolomeev et al. (2008) is that dual loss of both cIAP1 and cIAP2 severely attenuates TNFα -induced NF-κB activation, which leads to important questions regarding the individual functions of each protein. Due to the evidently crucial roles of both cIAP1 and 2 in the regulation of the NF-κB pathway coupled with the increasing evidence of NF-κB's involvement in muscle atrophy, our laboratory asked whether these IAPs could also potentially play a role in muscle wasting. Interestingly, our group recently demonstrated that the genetic ablation of cIAP1 protects against denervation-induced skeletal muscle atrophy in mice (Mrad et al., unpublished data). Of particular note, cIAP2 was found to be upregulated in the protected muscles of $cIAP1^{-/-}$ mice, leading us to hypothesize that perhaps cIAP2 was responsible for the protection seen in this model and as a result, could be considered to be a negative mediator of denervation-induced skeletal muscle atrophy.

1.7 TNF-like Weak Inducer of Apoptosis

Tumour necrosis factor (TNF)-like weak inducer of apoptosis (TWEAK) is a proinflammatory cytokine of the TNF superfamily (Chicheportiche et al., 1997). Although TWEAK was found not to be a particularly strong activator of apoptosis (Chicheportiche et al., 1997), this TNF family member has since been acknowledged as a potent muscle wasting cytokine that induces significant muscle atrophy when added to cultured myotubes or chronically administered in mice (Dogra et al., 2007). As a multifunctional cytokine, TWEAK has the ability to influence a number of cellular processes including proliferation, differentiation, migration, angiogenesis, apoptosis and inflammation (Leng et al., 2011; Winkles, 2008). This cytokine is broadly expressed in a number of tissues including the pancreas, heart, brain, intestine, ovary, skeletal muscle, vasculature, liver and kidney (Chicheportiche et al., 1997; Marsters et al., 1998). TWEAK exerts its function by trimerizing and binding to its receptor, fibroblast growth factor-inducible 14 (Fn14), after which signal transduction is promoted (Brown et al., 2003; Tran et al., 2005; Winkles et al., 2005; Saitoh et al., 2003). Fn14 is an inducible cell-surface receptor associated with a number of intracellular signalling pathways, including NF-κB (Meighan-Mantha et al., 1999; Feng et al., 2000). Upon activation and upregulation, Fn14 has the ability to activate the NF-κB pathway by signalling through a 28 amino acid cytoplasmic tail associated with TRAFs. Strikingly, this Fn14/TRAF complex is capable of inducing long-standing activation of NF-κB by means of biphasic induction of the canonical and noncanonical pathways (Burkly and Dohi, 2011; Saitoh et al., 2003).

Increasing evidence provides support for the hypothesis that the TWEAK/Fn14 system plays a role in normal tissue regeneration and repair following tissue injury, as verified in acute models of both liver and skeletal muscle injury (reviewed in Burkly and Dohi, 2011). When this pathway is dysregulated, however, the TWEAK/Fn14 system leads to progressive tissue damage along with maladaptive remodelling, as observed in inflammatory disease models (Burkly and Dohi, 2011). As stated previously, TWEAK has been identified as a potent muscle wasting cytokine (Dogra et al., 2007) and more recently the same group has elucidated the role of this cytokine in denervation-induced skeletal muscle atrophy (Mittal et al., 2010). The latter study demonstrated that with transgenic overexpression of TWEAK, the muscle atrophy that occurs as a consequence of sciatic nerve denervation is exacerbated, while this loss of muscle mass and function is rescued as a result of the genetic ablation of TWEAK. Mittal et al. (2010) were also able to establish that TWEAK in fact functions through NF-κB activation that leads to the upregulation of the MuRF1 E3 ligase in denervated skeletal muscle. This data coupled with previous evidence demonstrating the key role of the TWEAK/Fn14 system in mediating both inflammation and muscle wasting supports this pathway's key involvement in skeletal muscle atrophy and potentially in the model used in this particular research project.

With knowledge of the regulatory roles of both cIAP1 and cIAP2 in NF-κB activity, the involvement of NF-κB in muscle atrophy, along with the indication of TWEAK's function through the NF-κB pathway in atrophy, it can be hypothesized that each of these factors may possibly converge to form one of the potential mechanisms behind denervation-induced skeletal muscle atrophy.

1.8 Objectives

The goal of this research project is to investigate the role of cIAP2 in skeletal muscle atrophy in order to further understand the intricate mechanisms behind this debilitating disease state. Elucidating the mechanisms involved in muscle wasting may lead to treatment measures in the future, impacting on the quality of many lives. Specific research aims of this thesis include the characterization of the *in vivo* denervation model of atrophy in mice deficient in the cIAP2 gene, and the analysis of cIAP2-loss on the disuse phenotype. In addition, biochemical characterization of various markers of atrophy will also be performed in order to further support the phenotype observed following denervation.

I hypothesized that if cIAP2 is physiologically relevant in the protection of skeletal muscle against atrophy, then the genetic ablation of cIAP2 would result in an increase in muscle wasting that occurs as a result of denervation.
Remarkably, and perhaps initially unexpectedly, my results were found to be the exact opposite; that is, that the loss of cIAP2 led to a protective phenotype in the denervation-induced atrophy model.

2. Materials and Methods

2.1 Animal Models

2.1.1 C57BL/6 Mice

4-6 week old male C57BL/6 mice were chosen to use as control mice in this study. These mice were suitable controls as our cIAP2$^{-/-}$ mice (outlined below) were back-crossed with C57BL/6 mice when they were produced. The mice were obtained from Charles River Laboratories Inc., in Montreal, Canada and transferred into the University of Ottawa Animal Care and Veterinary Services Facility. They were housed and bred in proper accordance with the Institutional Animal Care and Use Committee guidelines and had *ad libitum* access to food pellets and filtered sterile water. Mice were selected based on both their age and genotype, and their right hind limbs were denervated by removing a 3-5mm portion of the sciatic nerve in the mid-thigh region while their contralateral limbs were used as control. Mice were sacrificed and tissue harvested 7, 14 and 28 days following denervation.

2.1.2 cIAP2$^{-/-}$ Mice

cIAP2$^{-/-}$ mice were generated as described by Conte et al., 2006. Genotypes were confirmed through PCR analysis using ear notch and tail snip DNA as well as through western blotting of spleen protein extracts and the RIAP1 antibody which detects both cIAP1 and cIAP2.

2.2 Protein and RNA Sources and Extraction

2.2.1 Denervation

The right hind limbs of both C57BL/6 and cIAP2$^{-/-}$ mice were prepared for surgery by making a 1 cm incision proximal to the knee on the lateral side of the right leg along the axis of the femur and isolating the sciatic nerve. A 3-6mm portion of the sciatic nerve was removed in order to prevent reinnervation. The left limb was used as a control limb for experimental purposes. Mice were sacrificed at 7, 14 and 28 days post-denervation by intra-peritoneal administration of 10% sodium pentobarbital in 0.9% sterile saline followed by cervical dislocation. Muscle tissue was carefully excised from both denervated and control limbs of the mice along with the spleen, and promptly flash frozen in dry ice cooled 2-methylbutane and stored in -80^{o}C until further processing.

2.2.2 Protein Extraction

Protein was extracted from TA, soleus, EDL and gastrocnemius control and denervated muscle tissue obtained from -80^{o}C storage. Muscle tissue was placed in 2 ml tubes and submerged in whole cell lysis buffer along supplemented with. The submerged tissue was homogenized using the Polytron tissue homogenizer at full speed for approximately 5-10 seconds, depending on the size of the sample. Samples were left to sit on ice for 30 minutes and then placed in a Hettich Mikro 20 Centrifuge for 20 minutes at 4^{o}C at 13,000 rpm. The supernatant was collected and stored at -80^{o}C until assayed.

Protein was extracted from WT and cIAP2$^{-/-}$ primary myotubes in a similar fashion as with the tissue. Cells were detached from cell culture plates using ice cold

whole cell lysis buffer and a disposable cell scraper. Cells were transferred into 1.5 ml tubes using a 1 ml insulin syringe and lysed by extracting and releasing the cell solution through the syringe tip back into the tube 10 times. Cell lysates were then analyzed for protein content using a standard BioRad Assay and stored at -80^{o}C for later use.

2.2.3 RNA Extraction

RNA was isolated from rodent gastrocnemius muscle samples using the RNeasy kit (Qiagen Inc., Missisauga, ON) according to the manufacturer's protocol. Muscle tissue was obtained from -80^{o}C storage and submerged in RLT buffer in quantities no larger than 30 mg each. Tissue was homogenized using the Polytron tissue homogenizer at full speed for approximately 5-10 seconds. RNA was eluted from spin column membranes into 50ul RNase-free water which was collected following the first column passage. RNA concentrations were determined using a spectrophotometer (Eppendorf Biophotometer, Hamburg, Germany) with an OD reading of 260 nm. Samples were stored at -80^{o}C until further use.

2.3 Fibre cross-sectional analysis

2.3.1 Tissue sectioning

Muscle tissue was collected at 7, 14 and 28 days post-denervation in preparation for histology by embedding the tissue in OCT compound and flash freezing in dry ice cooled 2-methylbutane. OCT-embedded tissue was sliced into 10 um cross-sections using a microtome cryostat with the inside temperature set at -20^{o}C. Sections were placed

directly onto histology slides, left to air dry for 1 hour and stored at -80^{o}C until further processing.

2.3.2 Haemotoxylin and Eosin staining

Muscle tissue sections obtained from -80^{o}C storage were air dried for 15 minutes at room temperature in preparation for H&E staining. Slides were next placed in a coplin jar filled with Mayer's haemotoxylin for 3 minutes, rinsed for 5 minutes in distilled water, stained in eosin for 80 seconds, and dipped in distilled water until the eosin no longer streaked. Following the rinse, slides were dipped 8 times in 95% ethanol followed by another 8 times in 100% ethanol, to dehydrate the tissue sections. Sections were then equilibrated by dipping the slides in xylenes 5 times each, and then mounted using permount solution and allowed to dry for 1 hour before analysis.

2.3.3 Measurement of Fibre Cross-Sectional Area

Control and denervated H&E stained slides were observed under an Axioskop light microscope and pictures were taken using a Zeiss digital camera in both black and white and colour modes at 20x magnification. Individual cross-sectional muscle fibres were traced and measured in um^2 using both Northern Eclipse and Image J software.

2.3.4 Data Analysis

CSA measurement data was transferred into Excel (Microsoft) and the frequency distribution of control and denervated sections from each individual animal in both

C57BL/6 and cIAP2$^{-/-}$ mice were calculated by determining the number of measurements that fell within the given area ranges. The average fibre CSA of each animal was also calculated using standard formulae and plotted +/- SEM with statistics generated using Prism 5.0 (GraphPad Software, San Diego, CA).

2.4 Immunohistochemical Analysis of Fibre Type Composition

2.4.1 Immunofluorescent Staining

Soleus muscle tissue sections were obtained from -80^{o}C storage and prepared for immunofluorescence by air-drying for 15 minutes at room temperature. Slides were then placed in a coplin jar, submerged in Phosphate-Buffered Saline (PBS) and incubated at room temperature with gentle agitation for 3 minutes. After removing slides from PBS, they were lightly shaken to eliminate any excess PBS from sections and immediately covered with primary antibody dilution (500 ul total solution per slide: 450 ul PBS-Triton, 50 ul goat serum, 5 ul anti-mouse MHC-fast antibody). Cover slips were placed over the antibody-covered slides to prevent evaporation and incubated at 4^{o}C over night in a humidified chamber. The following day, slides were obtained from 4^{o}C incubation and washed 3 times in PBS for 5 minutes each in a coplin jar. Sections were covered in 500 ul per slide of fluorescent secondary antibody dilution (490 ul PBS, 1 ul anti-mouse secondary antibody (Invitrogen), 10 ul DAPI). Cover slips were placed over the slides and incubated at room temperature for 1 hour in a humidified chamber protected from the light. Slides were then washed 3 times in PBS for 5 minutes each in the dark and anti-fade mounting reagent was applied to each slide, covered with cover slips, and allowed to dry for 1 hour in the dark prior to analysis. Slides were viewed under a fluorescent

microscope and pictures were taken with an Axioskop microscope and Zeiss camera to prepare for analysis.

2.4.2 Fibre Type Composition Analysis

The MHC antibody chosen for this experiment (Table 1) detects fast twitch or type II muscle fibres. Images were analyzed and fibres counted using ImageJ software. Red fluorescent labelled fibres were counted as type II, and those fibres not stained were counted as type I or other.

2.4.3 Data Analysis

Fibre count data was transferred into Excel (Microsoft) and the sums of control and denervated sections of solei muscles from each C57BL/6 and cIAP2$^{-/-}$ mice was calculated using standard formulae and plotted +/- SEM. Statistics were generated using Prism 5.0 (GraphPad Software, San Diego, CA).

2.5 Protein Level Analysis of TNF-like Weak Inducer of Apoptosis

2.5.1 ELISA Assay

Serum was collected 7 days post-denervation in 2 ml tubes and immediately centrifuged in a Hettich Mikro 20 Centrifuge for 20 minutes at 4^{o}C at 13,000 rpm. The supernatant was collected and stored in 1.5 ml tubes in -80^{o}C until assayed. TWEAK ELISA was carried out using a RayBio (Norcross, Georgia) Mouse Tweak ELISA Kit,

following the manufacturer's protocol. Each sample was run in triplicate and the mean absorbance in pg/ml was calculated using a SpectraMax (Molecular Devices) plate reader at a wavelength of 450 nm.

2.5.2 Data Analysis

Mean absorbance data collected from the TWEAK ELISA was transferred into Excel (Microsoft) and the overall average from both C57BL/6 and cIAP2$^{-/-}$ serum was calculated using standard formulae and plotted +/- SEM. Statistics were generated using Prism 5.0 (GraphPad Software, San Diego, CA), however, no there was no statistical significance to plot.

2.6 Polymerase Chain Reaction and Protein Analysis of Marker of Atrophy Genes

2.6.1 Quantitative Real-Time Reverse Transcriptase Polymerase Chain Reaction

For the analysis of Fn14 mRNA levels in response to denervation, RNA was extracted as previously described from *in vivo* models and samples were prepared for qRT-PCR analysis by obtaining RNA from -80^{o}C and allowing them to thaw on ice. Taqman real-time Reverse Transcriptase Polymerase Chain Reaction was carried out employing the use of endogenous GAPDH gene expression as a housekeeping gene. A master mix was prepared using QuantiTect SYBR Green RT-PCR reagents (Qiagen) according to the manufacturer's instructions and modified based on primer optimization.

2.6.2 Western Blot Analysis

Protein was extracted from *in vivo* and *in vitro* models as previously described and prepared for western blot analysis by removing from -80^{o}C storage and allowing to thaw on ice. As protein levels were determined by performing a standard BioRad assay on each sample, the concentrations were used to prepare samples containing 3.5-20 ug of protein and diluted 1:1 with 2x loading dye containing β-mercaptoethanol. Samples were loaded into wells of either 10 or 15 well polyacrylamide gels (10-15%) and run at 120 V for 1-1.5 hours.

Following the transfer of 1 hour at 400 mA, 0.5 um nitrocellulose membranes were blocked for 0.5 hours at room temperature with Odyssey blocking buffer. Membranes were washed with Tris-Phosphate Buffered Saline with Tween (TBS-T) for 45 minutes and promptly incubated with primary antibody overnight at room temperature. Each membrane was subsequently washed with TBS-T followed by incubation with species-specific fluorescent secondary antibody.

2.6 Effects of TWEAK on Primary Myotubes

2.6.1 Cell Culture

Primary myoblasts were prepared by euthanizing 4-6 week old female mice through cervical dislocation and dissecting the lower limb muscles. Cells were maintained in 10cm cell culture plates coated with 10% Matrigel (Sigma) and maintained in complete DMEM (ATCC) growth media supplemented with 10% horse serum (Invitrogen), 20% fetal bovine serum (Invitrogen), 10ng/ml FGF (Peprotech), 2ng/ml HGF (Peprotech) and

penicillin/streptomycin. Growth media was changed every 24 hours and cells passaged prior to reaching 80% confluence. It is of importance to note that cells were pre-plated on uncoated cell culture plates for 1 hour approximately every 2 passages in order to separate the fibroblasts from myoblasts and keep the culture as pure as possible.

Primary myoblasts were differentiated in DMEM supplemented with 10% equine serum for 48 hours. Myotubes were either left untreated for 24 hours, treated with 100 ng/ml of mouse recombinant TWEAK (Roche Applied Science) for 24 hours, or pre-treated for 0.5 hours with 500 nm SMC followed by treatment with 100 ng/ml of recombinant TWEAK for 24 hours. Pictures were taken using an Olympus microscope and camera.

Table 1. Primary Antibodies Used in Experiments

Antibody	Supplier	Host	Species Reactivity	Dilution
Anti-Gapdh	Advanced Immunochemicals	Mouse	Human, mouse, rat	1:10,000
Anti-RIAP1	Internally produced	Rabbit	Human, mouse, rat	1:2,000
Anti-RIAP3	Internally produced	Rabbit	Human, mouse, rat	1:5,000
Anti-p100/p52	Cell Signaling	Rabbit	Human, mouse, rat, monkey	1:1,000
Anti-MyoD	Santa Cruz M-318	Rabbit	Human, mouse, rat	1:1,000
Anti-MHC	Developmental Hybridoma Bank MF-20	Mouse	Mammalian, avian, amphibian	1:500
Anti-MHC-fast		Mouse		1:100
Anti-Laminin	Sigma Aldrich	Rabbit	Human, animal	1:500

3. Results

3.1 In Vivo Analysis of the Effects of the Loss of cIAP2 on Skeletal Muscle Atrophy

3.1.1 Denervation-Induced Skeletal Muscle Atrophy is Rescued by the Loss of cIAP2 7 Days Post-Denervation

To determine whether cIAP2 plays a role in skeletal muscle atrophy, I used the denervation model of disuse atrophy in cIAP2$^{-/-}$ mice and C57BL/6 controls. I denervated 4-6 week old C57BL/6 and cIAP2$^{-/-}$ mice by removing a 3-5mm portion of the sciatic nerve in the mid-thigh region of the lower right limb. The left limb was used for control purposes. Seven days later, TA muscle was harvested and tissue cross-sections were stained with H&E dyes (Fig. 3). Fibre CSA was analyzed by tracing each individual fibre and taking measurements of their area. A reduction in average fibre CSA is expected in muscle tissue following denervation. Also, a shift in fibre size occurs whereby the number of larger fibres decreases while the number of smaller fibres increases. To determine whether this shift occurs or is exacerbated in the absence of cIAP2, frequency distribution of fibre CSA was calculated in both non-denervated control (CTRL) and denervated (DEN) TA muscles of C57BL/6 and cIAP2$^{-/-}$ mice. As anticipated, C57BL/6 TA fibre measurements displayed a dramatic shift in fibre CSA from predominantly large fibres pre-denervation, toward a smaller fibre majority post-denervation (Fig 4a). However, cIAP2$^{-/-}$ TA did not exhibit this shift in frequency distribution, but instead, maintained their fibre size (Fig. 4b). Average CSA measurements confirmed that C57BL/6 TA decreased 42% compared to only 16% in cIAP2$^{-/-}$ TA. (Fig. 5). The same

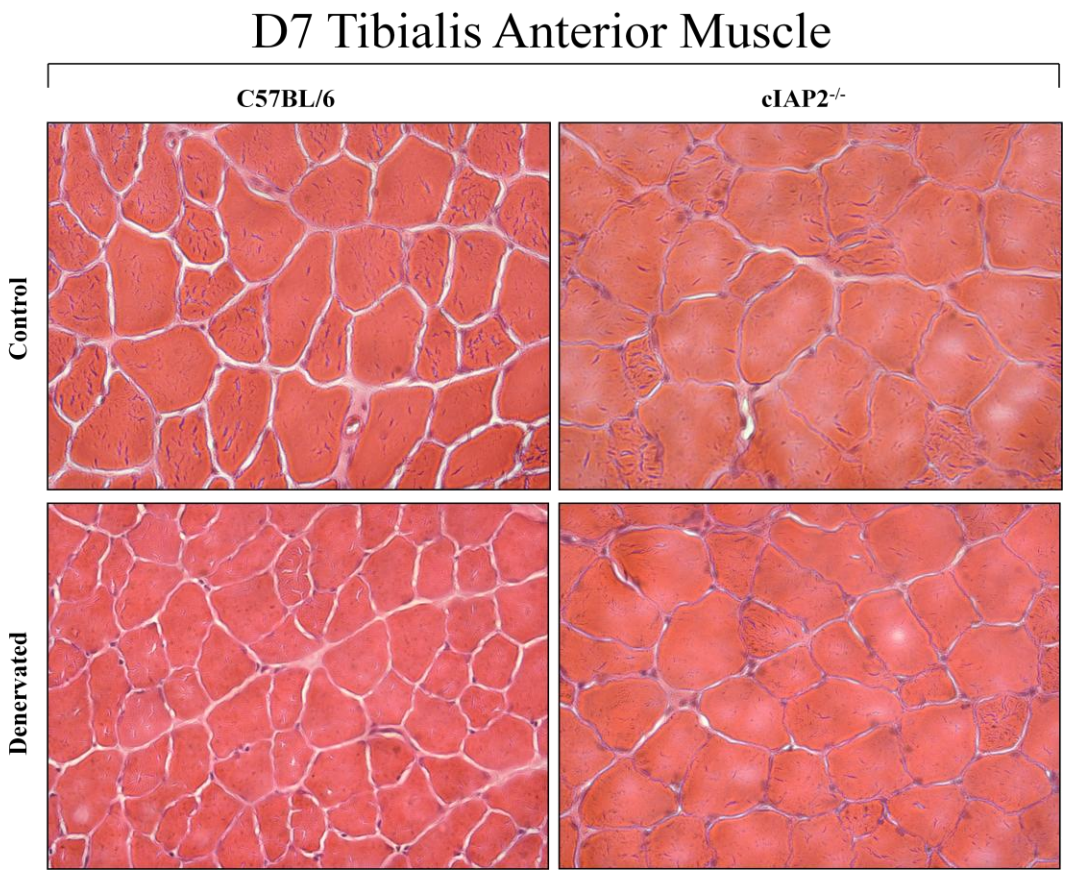

Figure 3. Absence of cIAP2 protects TA fibre cross-sectional area from denervation-induced atrophy 7 days post-denervation.

cIAP2$^{-/-}$ and C57BL/6 mice were denervated as described previously. Ten micrometer cross-sections were made of the TA muscle 7 days following denervation using a cryostat microtome and stained with haematoxylin and eosin. Images were taken using an Axioskop microscope and Northern Eclipse software.

A.

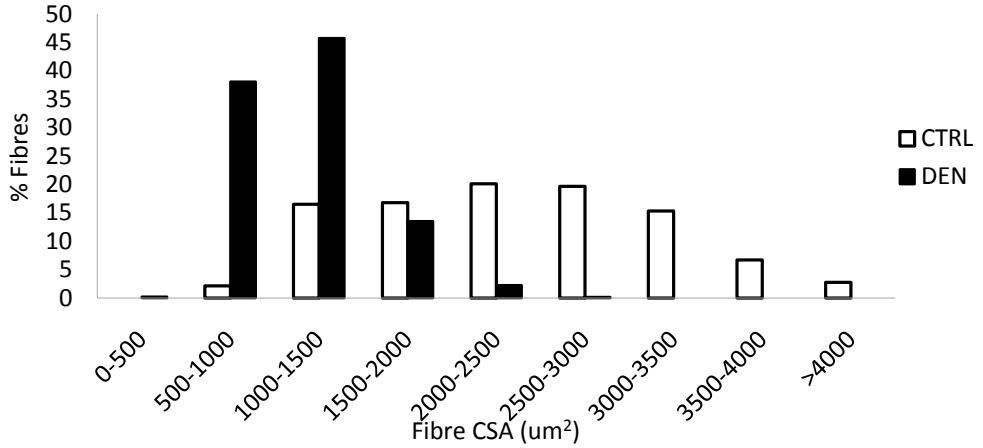

B.

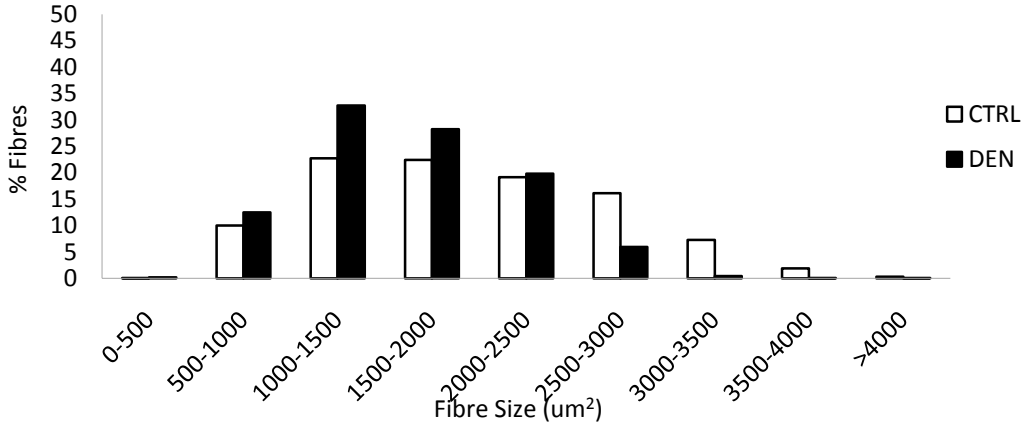

Figure 4. Fibre cross-sectional area fails to undergo a dramatic shift toward smaller fibres 7 days following denervation in cIAP2$^{-/-}$ TA compared to C57BL/6.

Fibre cross-sectional area was measured using haematoxylin and eosin stained sections of TA muscle collected from mice 7 days post denervation using Northern Eclipse and Image J software. I measured frequency distribution of fibre cross-sectional area in C57BL/6 (A) and cIAP2$^{-/-}$ (B) TA muscles. n=3 for each group.

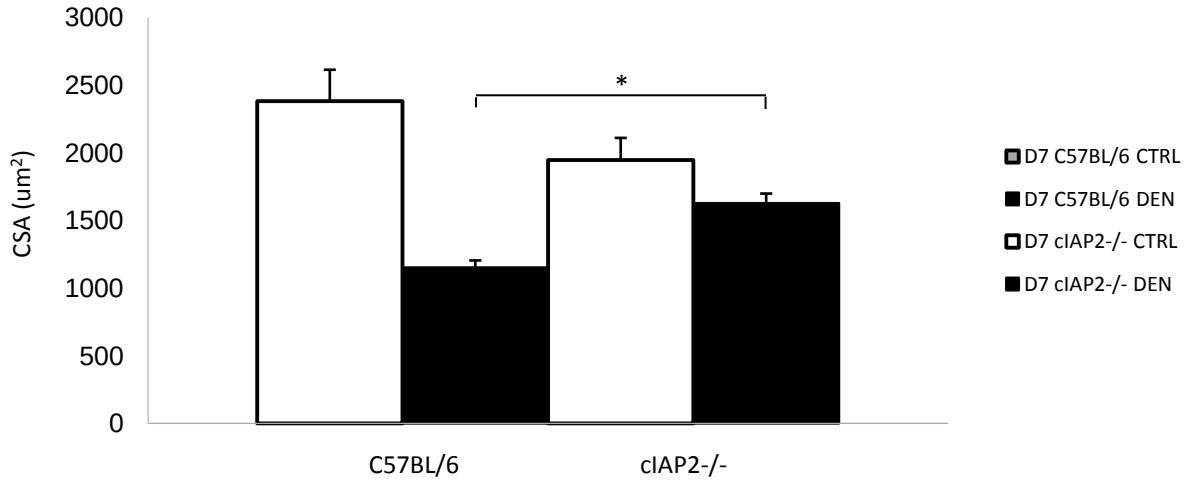

Figure 5. Fibre cross-sectional area is spared 7 days following denervation in cIAP2$^{-/-}$ TA compared to C57BL/6.

Fibre cross-sectional area was measured using haematoxylin and eosin stained sections of TA muscle collected from mice 7 days post denervation using Northern Eclipse and Image J software. The average cross-sectional area was calculated in both control and denervated limbs of C57BL/6 and cIAP2$^{-/-}$ TA. n=3 for each group. Values represent mean +/- standard error. * indicates significant difference, with $p < 0.01$.

analyses were performed on the SOL muscles (Fig. 6) and the results proved to be very similar to that of the TA. A significant shift in frequency distribution was observed in C57BL/6 mice (Fig.7a) compared to a maintenance of larger fibre size in cIAP2$^{-/-}$SOL (Fig. 7b). The average fibre CSA decreased by 59% in wild-type mice compared to only a 23% decrease in cIAP2$^{-/-}$ as a result of denervation (Fig. 8). The same analyses were also performed in EDL muscle. H&E stained photomicrographs revealed a significant protection in the DEN cIAP2$^{-/-}$ EDL when compared to C57BL/6 (Fig. 9), however, the protection seemed to be reduced when compared to that seen in both the TA and SOL muscles. Frequency distribution of fibre CSA measurements verified that in fact, the protection in cIAP2$^{-/-}$ EDL muscle was diminished compared to previous muscles analyzed, though the amount of atrophy was in fact still reduced. The expected shift in fibre CSA following denervation occurred in C57BL/6 EDL (Fig. 10a), yet there appeared to be a fairly substantial shift in fibre CSA in the cIAP2$^{-/-}$ mice as well (Fig. 10b), however with a larger number of fibres maintaining a greater area. C57BL/6 EDL displayed a 43% decrease in average fibre CSA following denervation, while fibres in cIAP2$^{-/-}$ EDL decreased in size by 35% (Fig. 11). Taken together, an overall conclusion can be made that 7 days following denervation, lower limb skeletal muscles are protected from denervation-induced muscle atrophy in the absence of cIAP2.

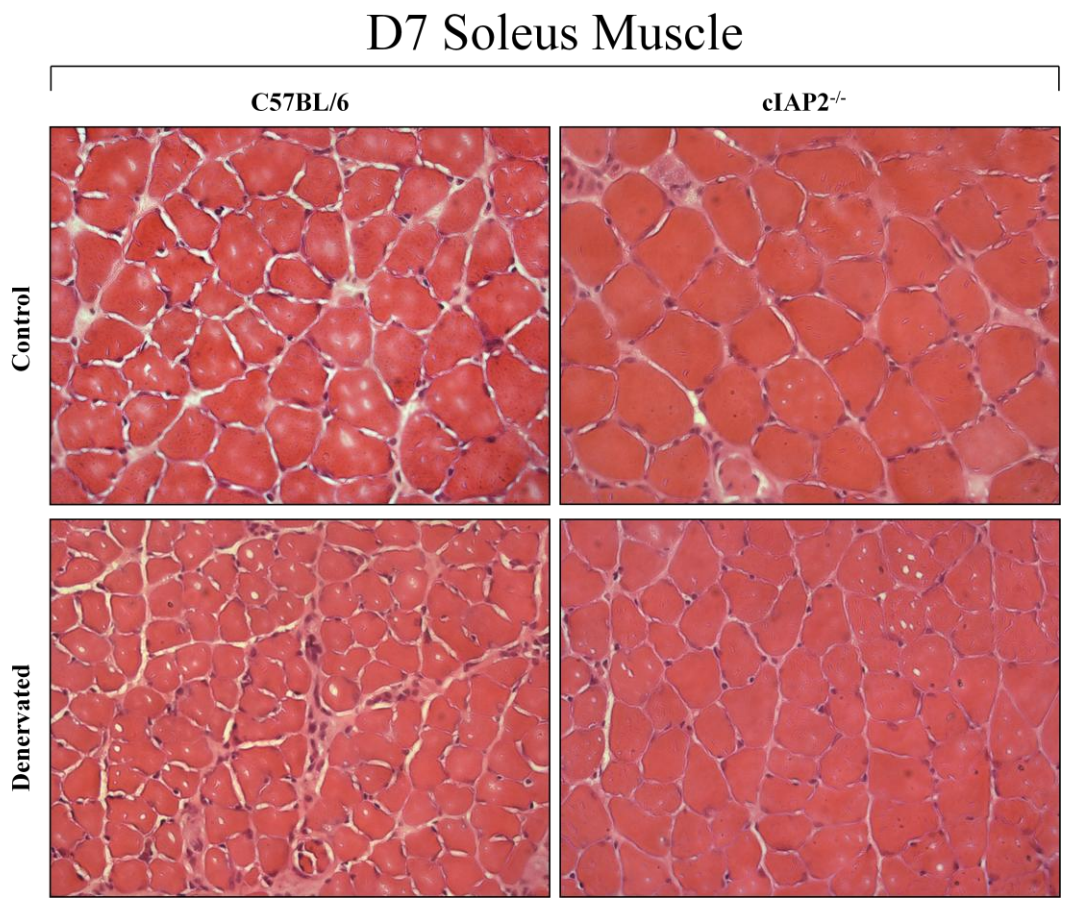

Figure 6. Absence of cIAP2 protects SOL fibre cross-sectional area from denervation-induced atrophy 7 days post-denervation.

cIAP2$^{-/-}$ and C57BL/6 mice were denervated as described previously. Ten micrometer cross-sections were made of the SOL muscle 7 days following denervation using a cryostat microtome and stained with haematoxylin and eosin. Images were taken using an Axioskop microscope and Northern Eclipse software.

A.

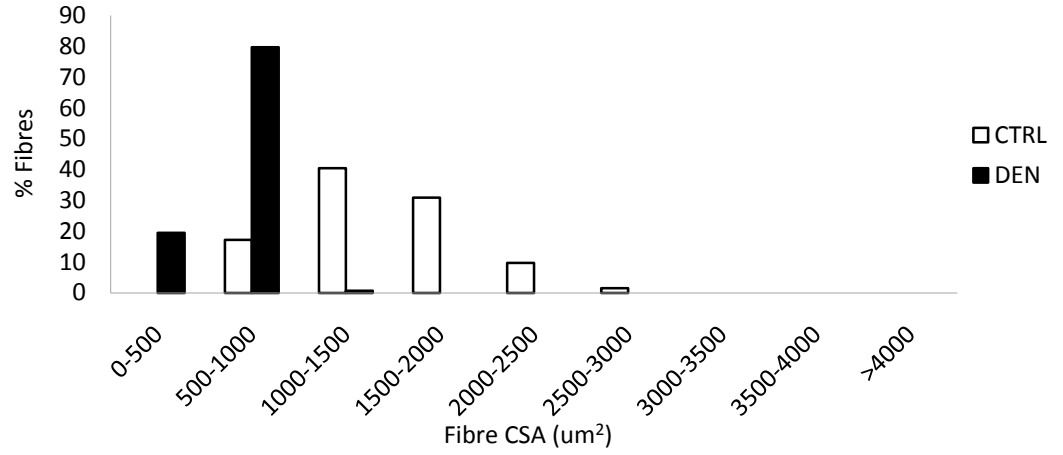

B.

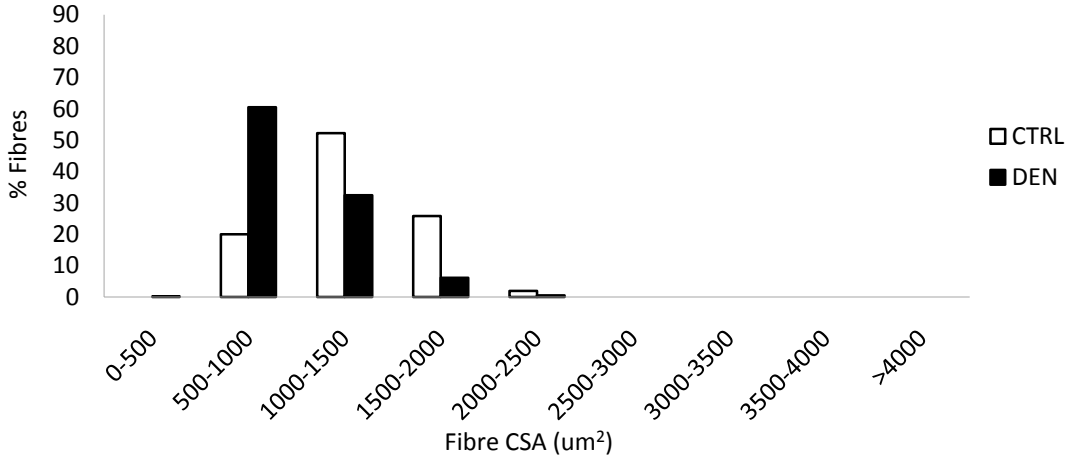

Figure 7. Fibre cross-sectional area fails to undergo a dramatic shift toward smaller fibres 7 days following denervation in cIAP2$^{-/-}$ SOL compared to C57BL/6.

Fibre cross-sectional area was measured using haematoxylin and eosin stained sections of SOL muscle collected from mice 7 days post denervation using Northern Eclipse and Image J software. I measured frequency distribution of fibre cross-sectional area in C57BL/6 (A) and cIAP2$^{-/-}$ (B) SOL muscles. n=3 for each group.

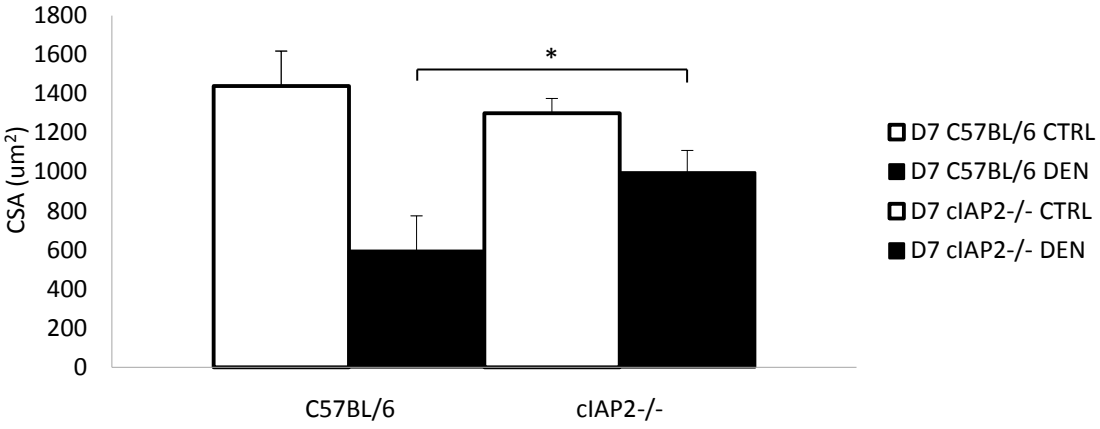

Figure 8. Fibre cross-sectional area is spared 7 days following denervation in cIAP2$^{-/-}$ SOL compared to C57BL/6.

Fibre cross-sectional area was measured using haematoxylin and eosin stained sections of SOL muscle collected from mice 7 days post denervation using Northern Eclipse and Image J software. The average cross-sectional area was calculated in both control and denervated limbs of C57BL/6 and cIAP2$^{-/-}$ SOL. n=3 for each group. Values represent mean +/- standard error. * indicates significant difference, with $p < 0.01$.

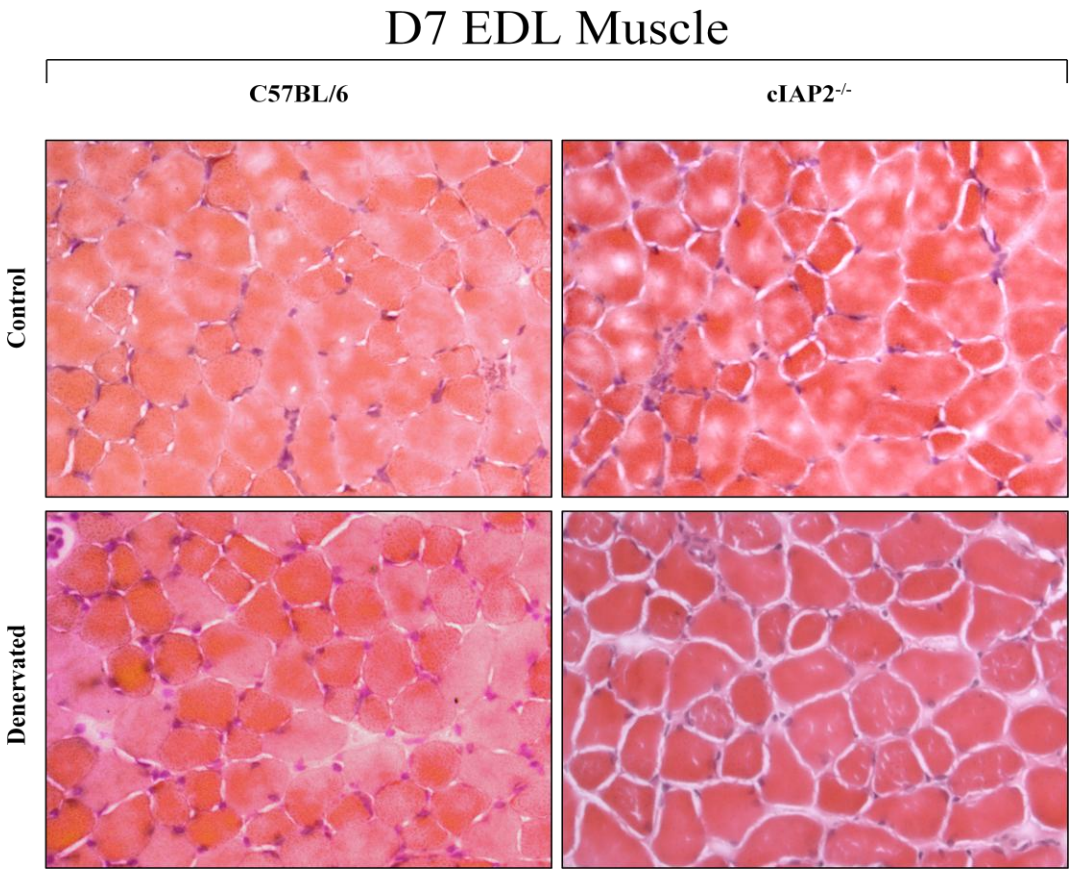

Figure 9. Absence of cIAP2 protects EDL fibre cross-sectional area from denervation-induced atrophy 7 days post-denervation.

cIAP2$^{-/-}$ and C57BL/6 mice were denervated as described previously. Ten micrometer cross-sections were made of the EDL muscle 14 days following denervation using a cryostat microtome and stained with haematoxylin and eosin. Images were taken using an Axioskop miscroscope and Northern Eclipse software.

A.

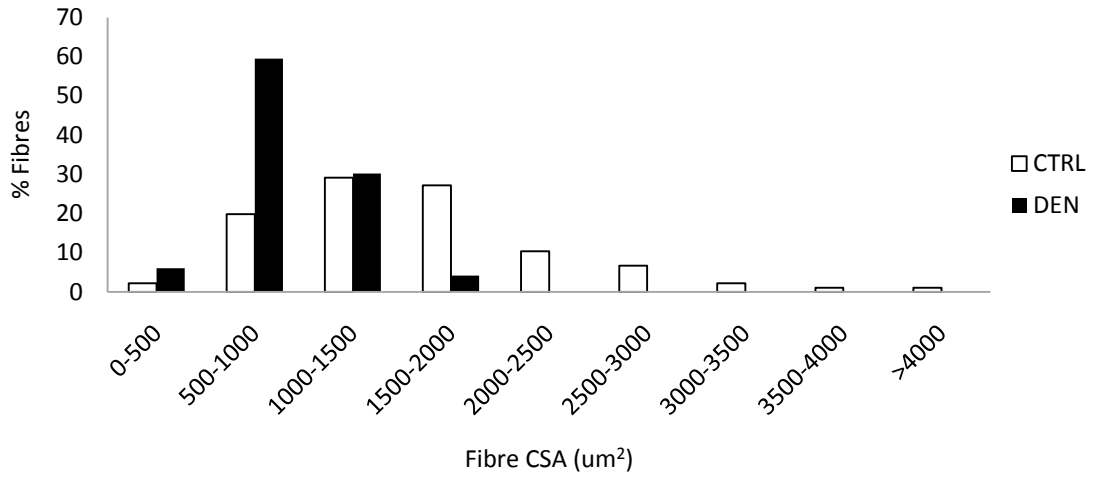

B.

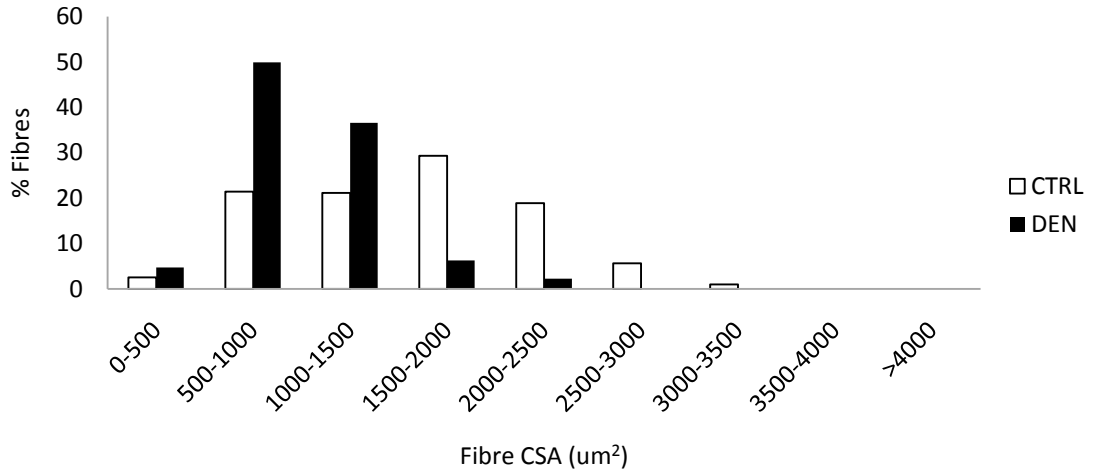

Figure 10. Fibre cross-sectional area fails to undergo a dramatic shift toward smaller fibres 7 days following denervation in cIAP2$^{-/-}$ EDL compared to C57BL/6.

Fibre cross-sectional area was measured using haematoxylin and eosin stained sections of EDL muscle collected from mice 7 days post denervation using Northern Eclipse and Image J software. I measured frequency distribution of fibre cross-sectional area in C57BL/6 (A) and cIAP2$^{-/-}$ (B) EDL muscles. n=2 for each group.

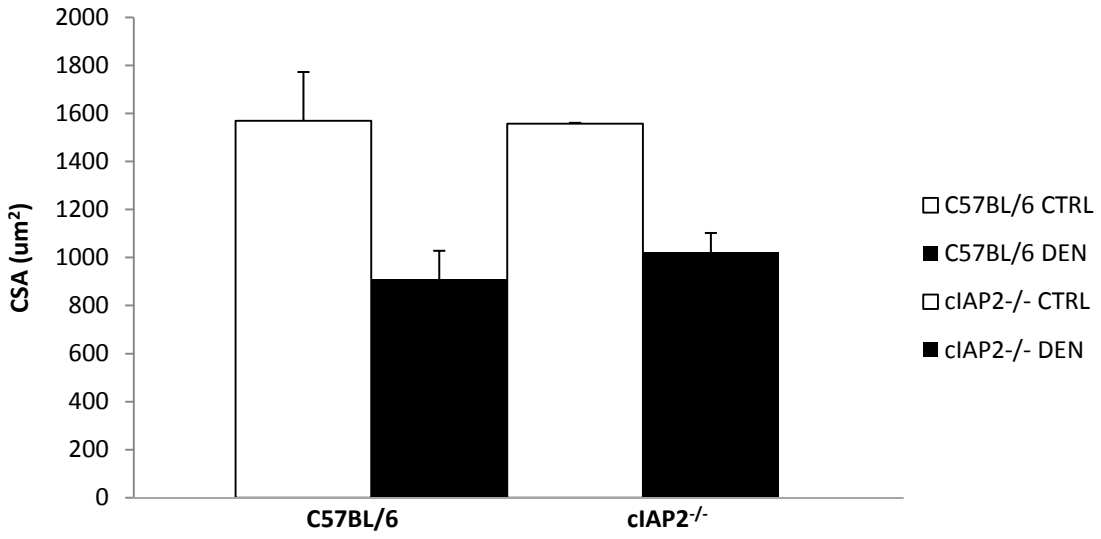

Figure 11. Fibre cross-sectional area is spared 7 days following denervation in cIAP2$^{-/-}$ EDL compared to C57BL/6.

Fibre cross-sectional area was measured using haematoxylin and eosin stained sections of EDL muscle collected from mice 7 days post denervation using Northern Eclipse and Image J software. The average cross-sectional area was calculated in both control and denervated limbs of C57BL/6 and cIAP2$^{-/-}$ EDL. n=2 for each group. Values represent mean +/- standard error.

3.1.2 Protection Against Denervation-Induced Skeletal Muscle Atrophy is Maintained 14 Days Post-Denervation

To further examine the effect of cIAP2-loss on denervation atrophy, I analyzed muscle samples from 14 days following denervation. At this time point, protection was still evident in cIAP2$^{-/-}$ TAs as compared to controls (Fig. 12). Specifically, the cIAP2$^{-/-}$ TAs failed to exhibit the shifts in fibre size distribution that were clearly manifested in the C57BL/6 controls (Fig. 13). Furthermore, a 14-day denervation saw the average CSA decrease by 57% in the C57BL/6 TAs, as compared to only 27% in cIAP2$^{-/-}$ (Fig. 14); in essence, the extent of atrophy was reduced by half in the absence of cIAP2. cIAP2$^{-/-}$ SOL muscles also appeared to show the same extent of protection as that of the TAs, observed by H&E stained photomicrographs (Fig. 15). Correspondingly, the fibre CSA frequency distribution calculations of solei from both C57BL/6 (Fig. 17a) and cIAP2$^{-/-}$ (Fig. 16b) mice displayed similar results to that seen at 7 days post-denervation. C57BL/6 DEN SOL fibres underwent the expected shift in fibre CSA to an overall smaller average size, whereas cIAP2$^{-/-}$ SOL fibre CSA was largely preserved. These results were in full support of the protection observed in cIAP2$^{-/-}$ H&E stained SOL sections. In addition, average fibre CSA measurements further confirmed this protection as cIAP2$^{-/-}$ SOL fibre CSA only decreased by 26% following denervation, compared to a more significant 46% in C57BL/6 (Fig. 17). Interestingly, the H&E stained photomicrographs of cIAP2$^{-/-}$ EDL displayed a more obvious protection against atrophy than that observed 7 days after denervation (Fig. 18). Fibre CSA frequency distribution graphs demonstrated a clear reduction in the number of larger fibres found in C57BL/6 DEN EDL (Fig. 19a) whereas a higher number of fibres maintained their size in cIAP2$^{-/-}$ EDL (Fig. 19b). Average fibre

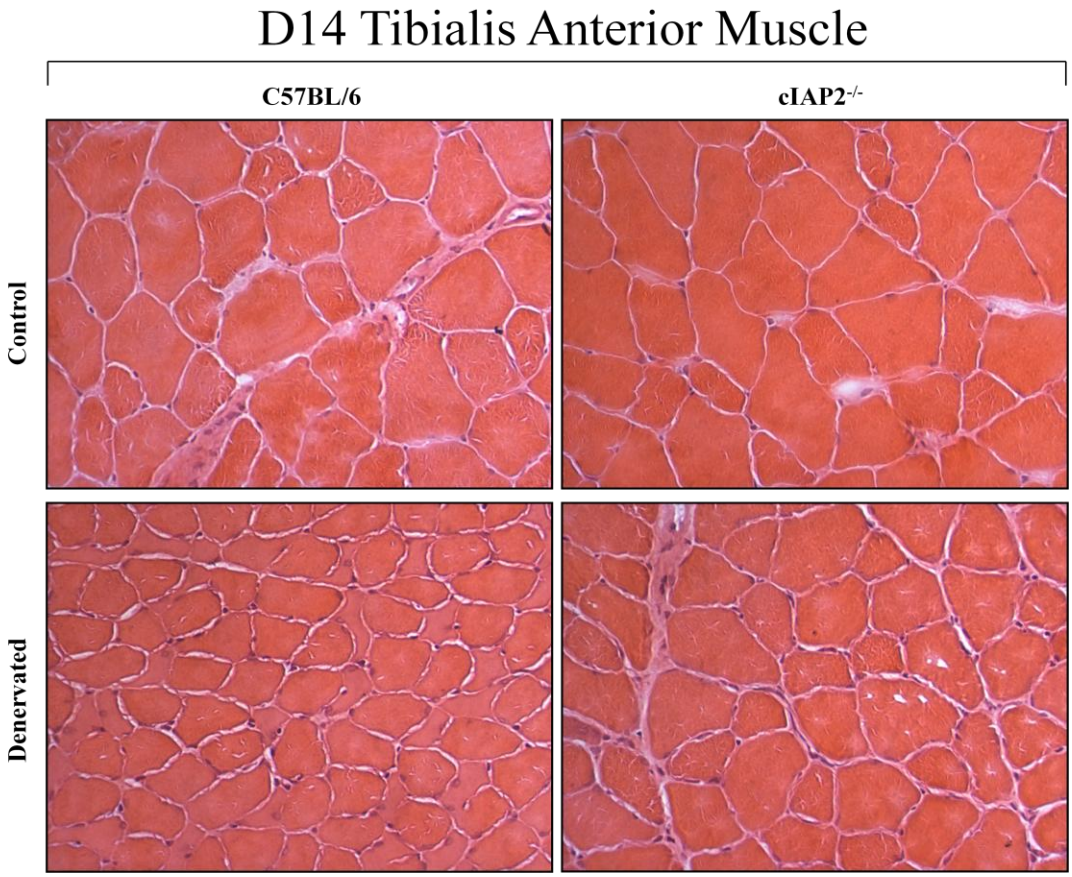

Figure 12. Absence of cIAP2 protects TA fibre cross-sectional area from denervation-induced atrophy 14 days post-denervation.

cIAP2$^{-/-}$ and C57BL/6 mice were denervated as described previously. Ten micrometer cross-sections were made of the TA muscle 14 days following denervation using a cryostat microtome and stained with haematoxylin and eosin. Images were taken using an Axioskop microscope and Northern Eclipse software.

A.

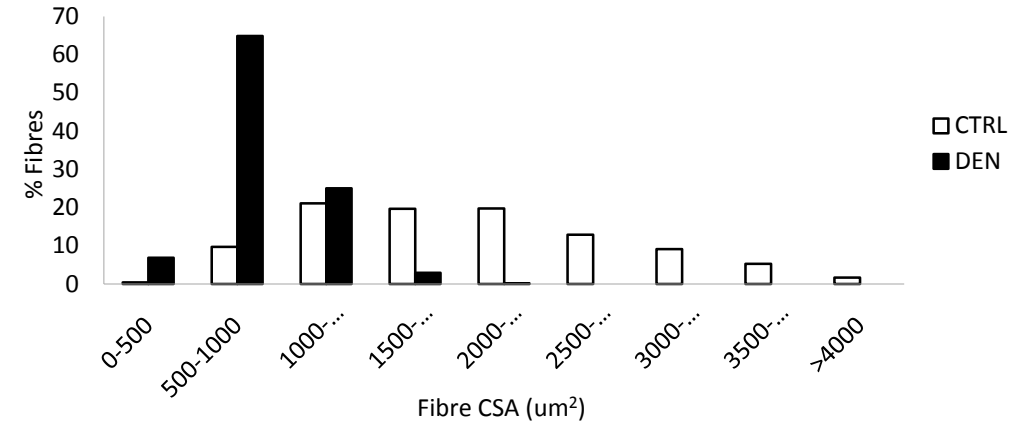

B.

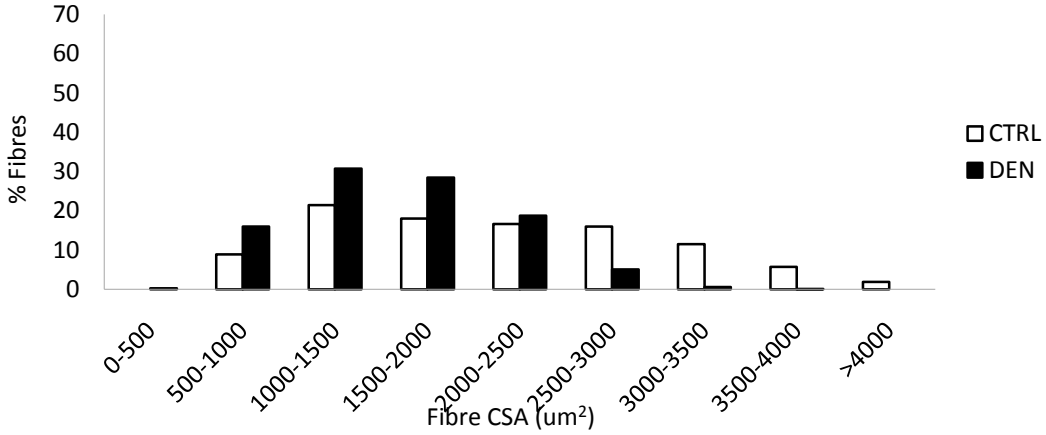

Figure 13. Fibre cross-sectional area fails to undergo a dramatic shift toward smaller fibres 14 days following denervation in cIAP2$^{-/-}$ TA compared to C57BL/6.

Fibre cross-sectional area was measured using haematoxylin and eosin stained sections of TA muscle collected from mice 14 days post denervation using Northern Eclipse and Image J software. I measured frequency distribution of fibre cross-sectional area in C57BL/6 (a) and cIAP2$^{-/-}$ (b) TA muscles. n=3 for each group.

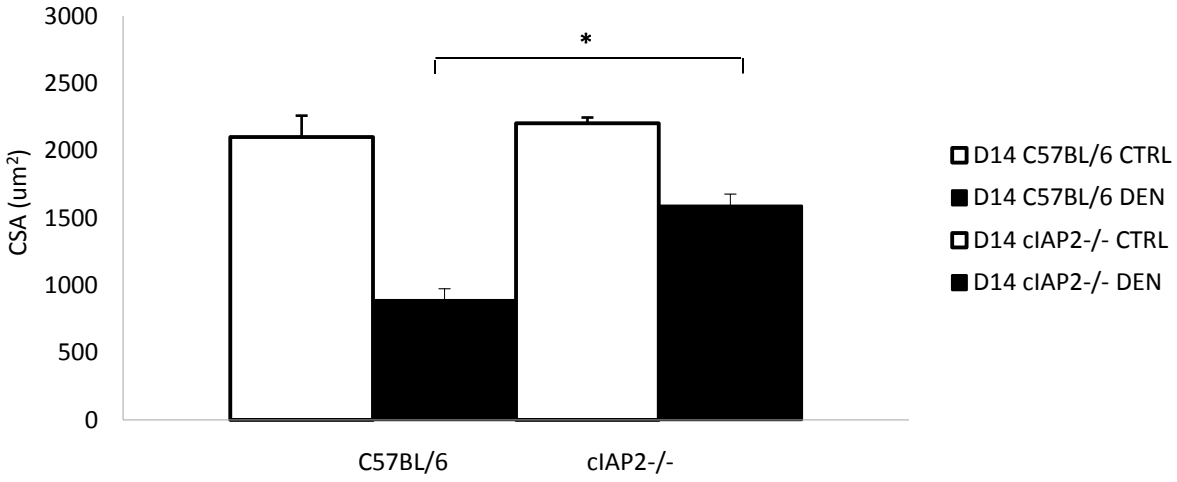

Figure 14. Fibre cross-sectional area is spared 14 days following denervation in cIAP2$^{-/-}$ TA compared to C57BL/6.

Fibre cross-sectional area was measured using haematoxylin and eosin stained sections of TA muscle collected from mice 14 days post denervation using Northern Eclipse and Image J software. The average cross-sectional area was calculated in both control and denervated limbs of C57BL/6 and cIAP2$^{-/-}$ TA. n=3 for each group. Values represent mean +/- standard error. * indicates significant difference, with $p < 0.01$

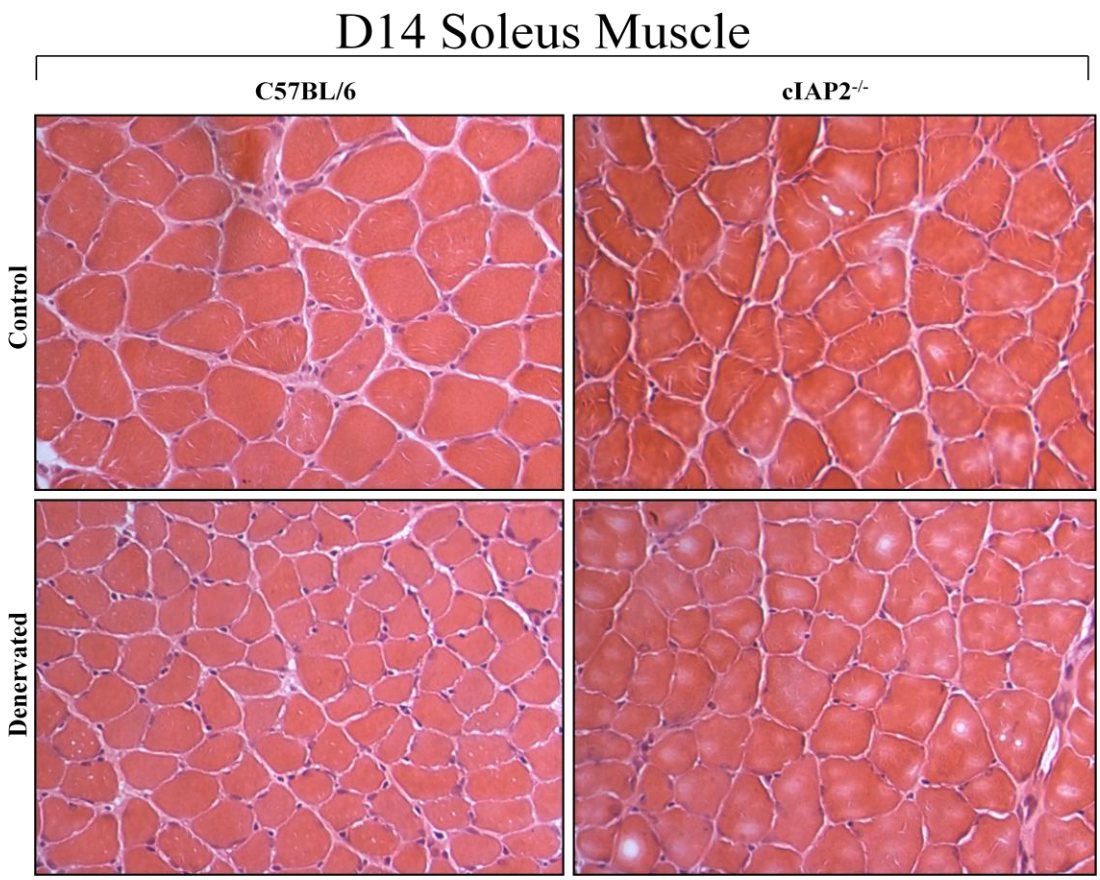

Figure 15. Absence of cIAP2 protects SOL fibre cross-sectional area from denervation-induced atrophy 14 days post-denervation.

cIAP2$^{-/-}$ and C57BL/6 mice were denervated as described previously. Ten micrometer cross-sections were made of the SOL muscle 14 days following denervation using a cryostat microtome and stained with haematoxylin and eosin. Images were taken using an Axioskop miscroscope and Northern Eclipse software.

A.

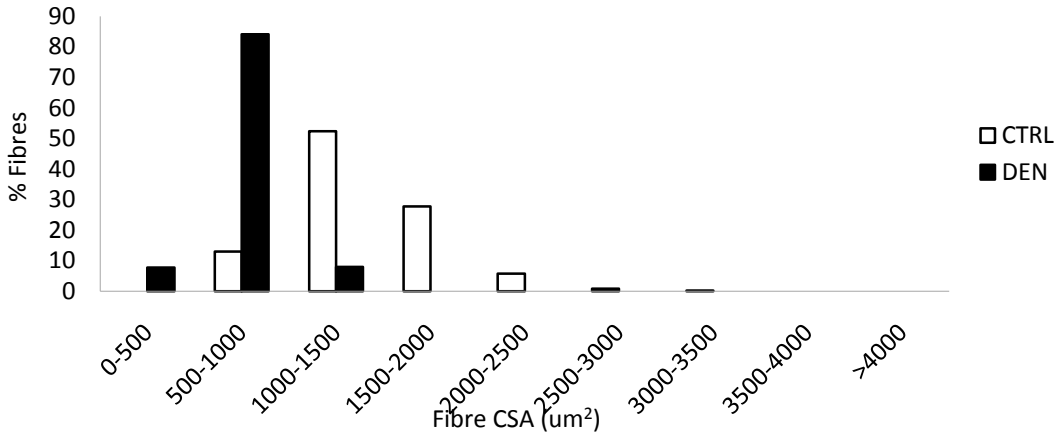

B.

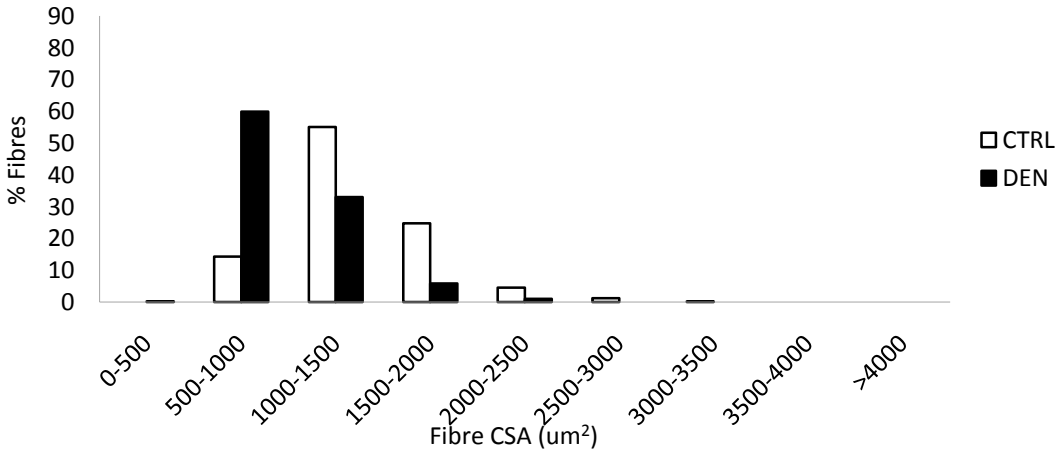

Figure 16. Fibre cross-sectional area fails to undergo a dramatic shift toward smaller fibres 14 days following denervation in cIAP2$^{-/-}$ SOL compared to C57BL/6.

Fibre cross-sectional area was measured using haematoxylin and eosin stained sections of SOL muscle collected from mice 14 days post denervation using Northern Eclipse and Image J software. I measured frequency distribution of fibre cross-sectional area in C57BL/6 (A) and cIAP2$^{-/-}$ (B) SOL muscles. n=3 for each group.

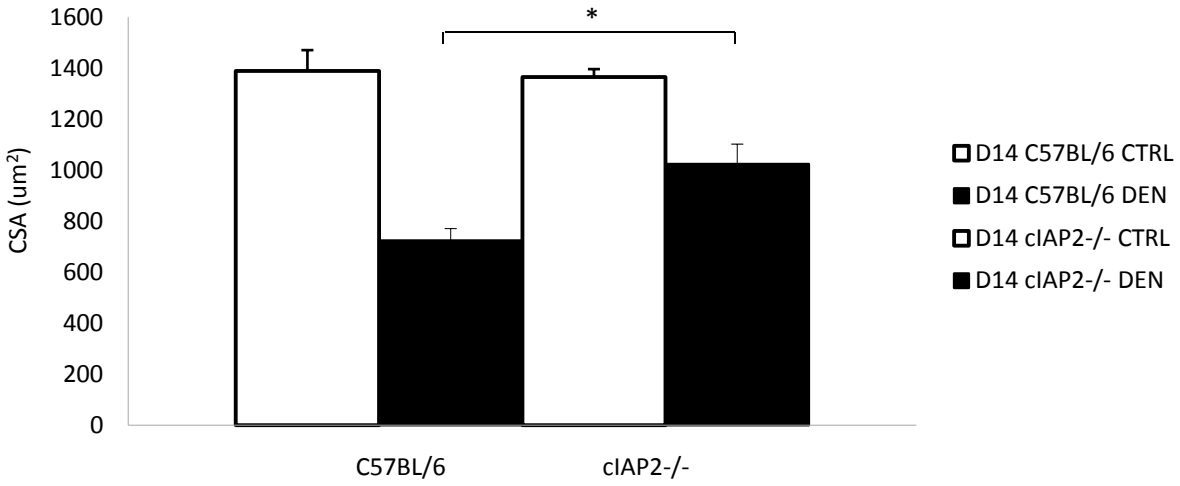

Figure 17. Fibre cross-sectional area is spared 14 days following denervation in cIAP2$^{-/-}$ SOL compared to C57BL/6.

Fibre cross-sectional area was measured using haematoxylin and eosin stained sections of SOL muscle collected from mice 14 days post denervation using Northern Eclipse and Image J software. The average cross-sectional area was calculated in both control and denervated limbs of C57BL/6 and cIAP2$^{-/-}$ SOL. n=3 for each group. Values represent mean +/- standard error. * indicates significant difference, with $p < 0.01$.

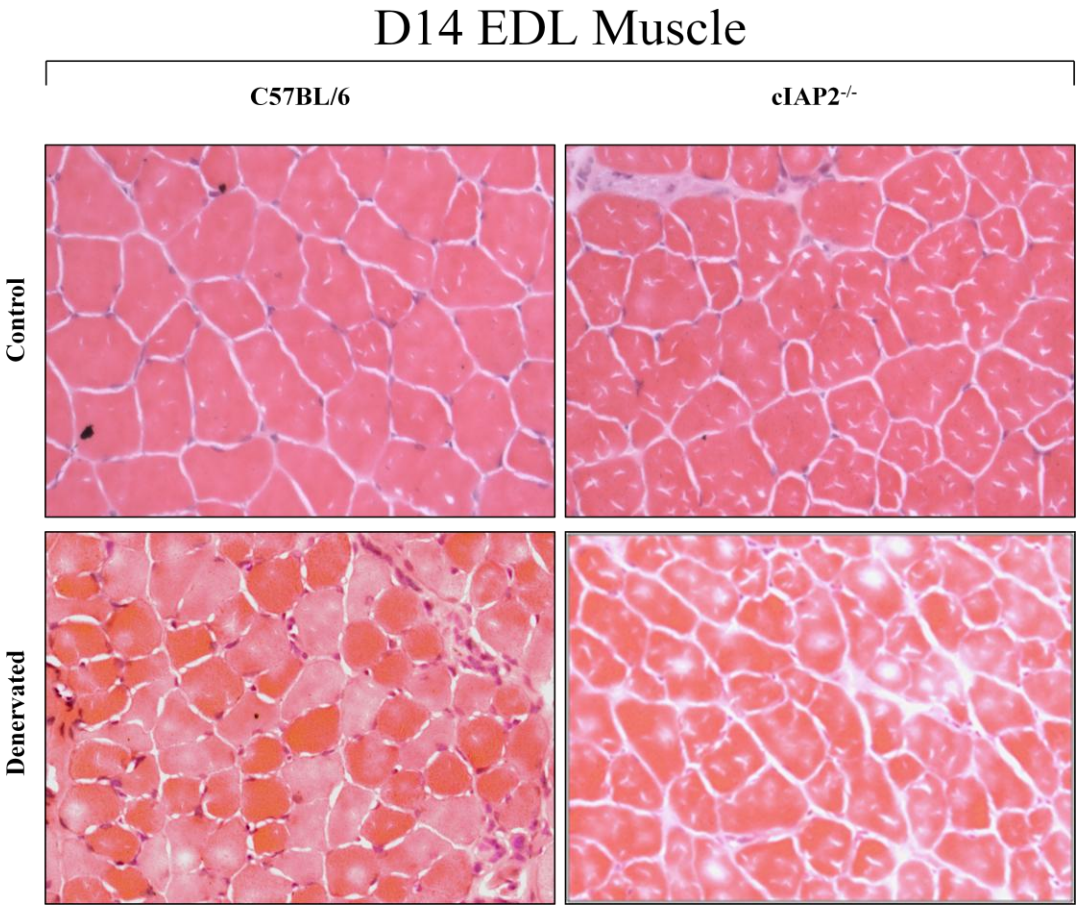

Figure 18. Absence of cIAP2 protects EDL fibre cross-sectional area from denervation-induced atrophy 14 days post-denervation.

cIAP2$^{-/-}$ and C57BL/6 mice were denervated as described previously. Ten micrometer cross-sections were made of the EDL muscle 14 days following denervation using a cryostat microtome and stained with haematoxylin and eosin. Images were taken using an Axioskop miscroscope and Northern Eclipse software.

A.

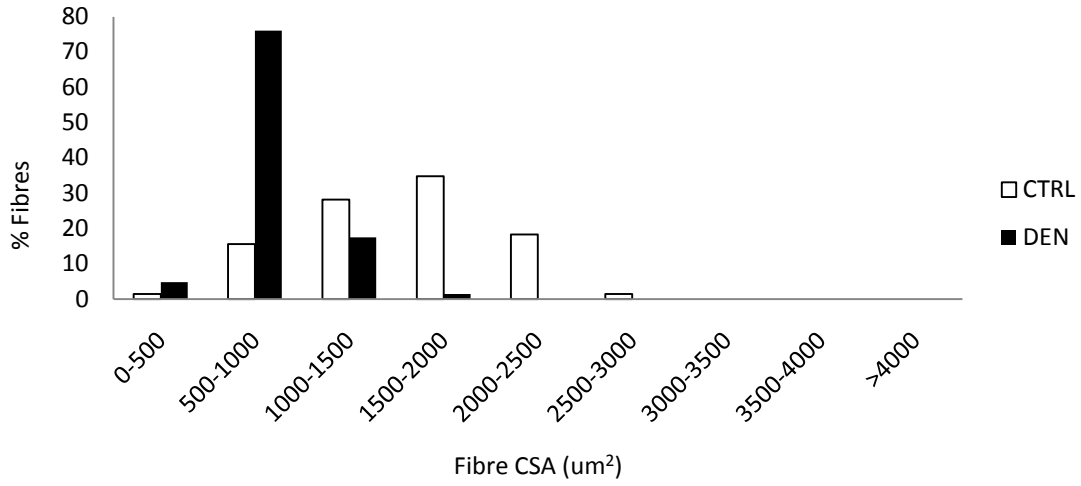

B.

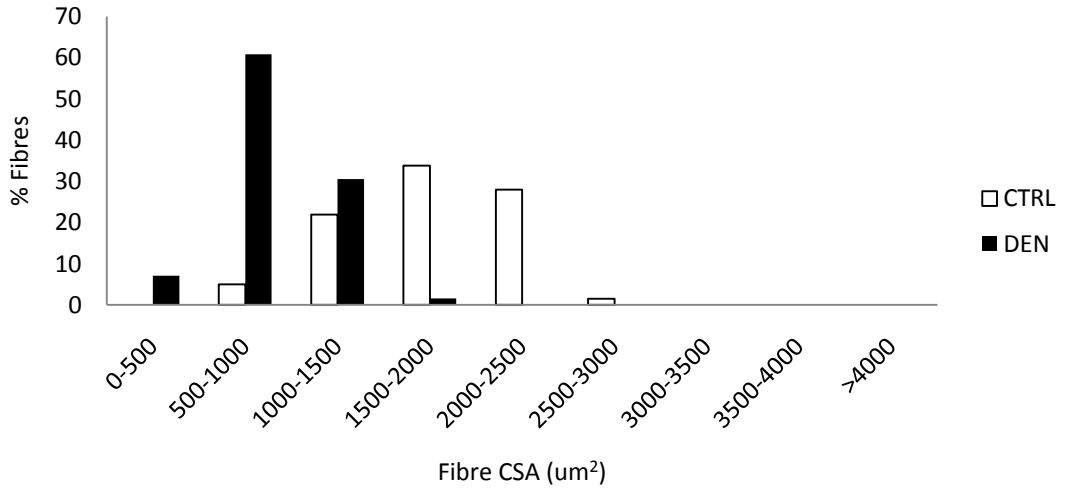

Figure 19. Fibre cross-sectional area fails to undergo a dramatic shift toward smaller fibres 14 days following denervation in cIAP2$^{-/-}$ EDL compared to C57BL/6.

Fibre cross-sectional area was measured using haematoxylin and eosin stained sections of EDL muscle collected from mice 14 days post denervation using Northern Eclipse and Image J software. I measured frequency distribution of fibre cross-sectional area in C57BL/6 (A) and cIAP2$^{-/-}$ (B) EDL muscles. n=2 for C57BL/6 group; n=3 for cIAP2$^{-/-}$ group.

CSA measurements, however, clearly displayed the EDL's protection against denervation-induced atrophy in cIAP2$^{-/-}$ mice. These data displayed an evident preservation of fibre size in cIAP2$^{-/-}$ EDL with a 34% reduction in CSA following denervation, compared to a decrease of 46% in C57BL/6 fibre CSA (Fig. 20). Taken together, these results provide sufficient evidence for the significant effects of the absence of cIAP2 on skeletal muscle atrophy in the TA, SOL, and EDL muscles. In particular, the protection against denervation-induced atrophy that occurs as a result of the loss of this gene is quite considerable, and is sustained, if not more pronounced, 14 days following nerve injury.

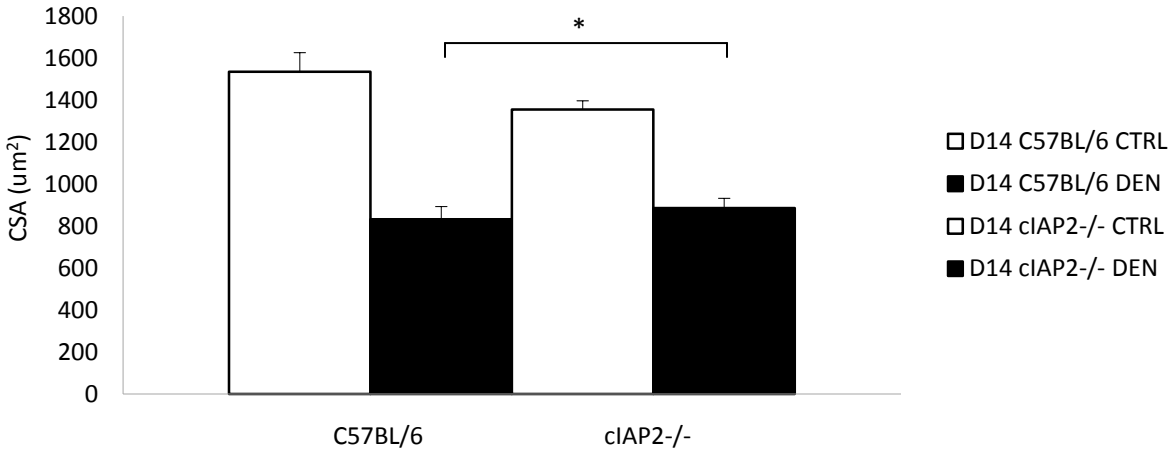

Figure 20. Fibre cross-sectional area is spared 14 days following denervation in cIAP2$^{-/-}$ EDL compared to C57BL/6.

Fibre cross-sectional area was measured using haematoxylin and eosin stained sections of EDL muscle collected from mice 7 days post denervation using Northern Eclipse and Image J software. The average cross-sectional area was calculated in both control and denervated limbs of C57BL/6 and cIAP2$^{-/-}$ EDL. n=2 for C57BL/6 group; n=3 for cIAP2$^{-/-}$ group. Values represent mean +/- standard error. * indicates significant difference, with $p < 0.05$.

3.1.3 Fibre Size Maintenance is Diminished 28 Days after Denervation in the Absence of cIAP2

After determining that the deletion of cIAP2 results in a significant preservation in skeletal muscle against atrophy at both 7 and 14 days post-denervation, I asked whether this protection would be maintained after 28 days of disuse. To determine whether cIAP2$^{-/-}$ mice still exhibited this protection after 4 weeks of disuse, I denervated the animals and excised the TA muscles 28 days later. Fibre CSA was measured using H&E stained sections from both C57BL/6 and cIAP2$^{-/-}$ mice. Fibre size distribution calculations demonstrated that cIAP2$^{-/-}$ TA (Fig. 21b) maintained their fibre CSA to a lesser degree than at 7 and 14 days post-denervation. Nonetheless, they did exhibit a protection against atrophy compared to C57BL/6 (Fig. 21a). Furthermore, average fibre CSA measurements supported the frequency distribution results as C57BL/6 TA fibre CSA decreased 68% in size after denervation, compared to a 48% decrease in cIAP2$^{-/-}$ TA (Fig. 22). These results suggest that the preservation in skeletal muscle of CIAP2$^{-/-}$ mice is most substantial during 7 and 14 day periods of disuse, while this level of protection diminishes after 28 days.

A.

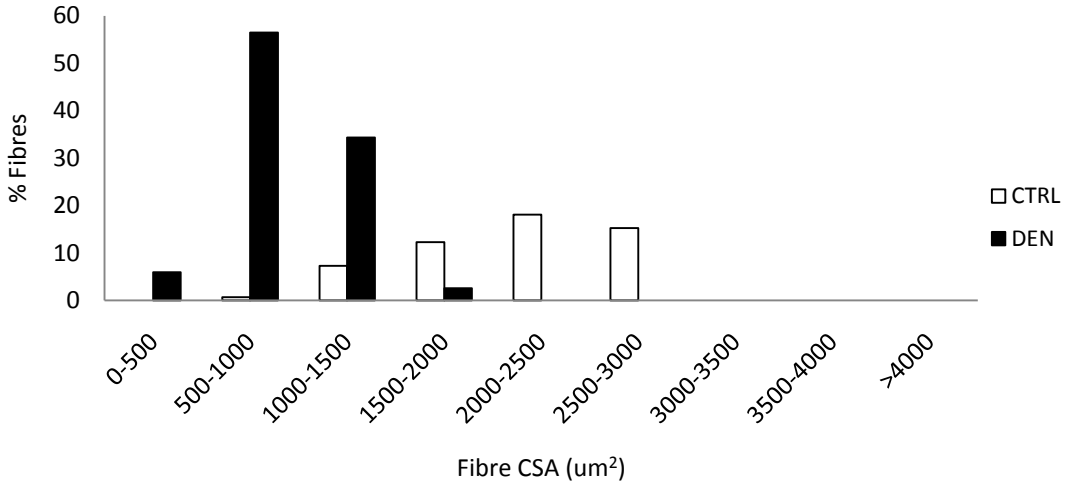

B.

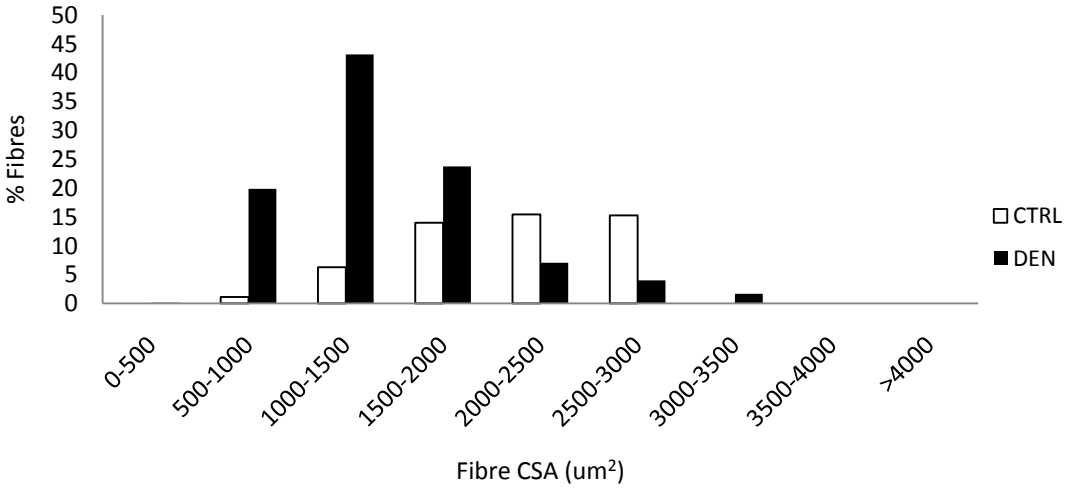

Figure 21. Fibre cross-sectional area fails to undergo a dramatic shift toward smaller fibres 28 days following denervation in cIAP2$^{-/-}$ TA compared to C57BL/6.

Fibre cross-sectional area was measured using haematoxylin and eosin stained sections of TA muscle collected from mice 28 days post denervation using Northern Eclipse and Image J software. I measured frequency distribution of fibre cross-sectional area in C57BL/6 (A) and cIAP2$^{-/-}$ (B) TA muscles. n=2 for C57BL/6 group; n=3 for cIAP2$^{-/-}$ group.

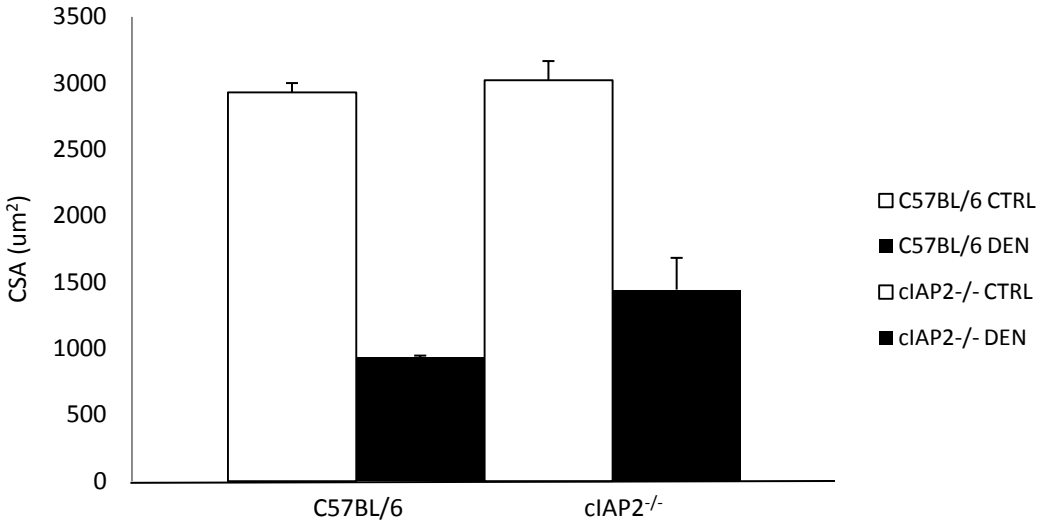

Figure 22. Fibre cross-sectional area is spared 28 days following denervation in cIAP2$^{-/-}$ TA compared to C57BL/6.

Fibre cross-sectional area was measured using haematoxylin and eosin stained sections of TA muscle collected from mice 28 days post denervation using Northern Eclipse and Image J software. The average cross-sectional area was calculated in both control and denervated limbs of C57BL/6 and cIAP2$^{-/-}$ TA. n=2 for C57BL/6 group; n=3 for cIAP2$^{-/-}$ group. Values represent mean +/- standard error.

3.1.4 Analysis of Various Markers of Atrophy and IAP Expression by Western Blot Analysis

The evidence so far suggests that the genetic ablation of cIAP2 results in a protection against atrophy. To establish whether biochemical analyses support these results, Western blotting analysis was performed to determine the protein levels of a number of markers of atrophy and the IAPs, in response to denervation. Although a role for the IAPs in atrophy has not yet been established, our laboratory has found that both the X-linked inhibitor of apoptosis (XIAP) and cIAP1 are consistently induced in response to denervation, as observed by western blot analysis. XIAP can be detected by the RIAP3 antibody while cIAP1 is detected using the RIAP1 antibody (see Table 1 and Figure 24, for example). RIAP1 is capable of detecting both cIAP1 and cIAP2 simultaneously, although the separation of the bands is only 2 kDa. These two proteins can sometimes be quite difficult to distinguish; however, cIAP2 has been documented to not be expressed in muscle tissue (Mahoney et al., 2008). Therefore, it can be assumed that the product observed from probing cIAP2$^{-/-}$ muscle samples with RIAP1 is cIAP1. To investigate the expression levels of each XIAP and cIAP1 in CTRL and DEN muscle samples of C57BL/6 and cIAP2$^{-/-}$ animals, gastrocnemius (GAS) lysates were probed with both RIAP3 and RIAP1 antibodies. Basal levels of XIAP appeared to be lower in CTRL cIAP2$^{-/-}$ GAS than in C57BL/6, at both 7 (Fig. 23a, top panel) and 14 days (Fig. 24, 3rd panel from top) post-denervation. XIAP expression did, however, increase after denervation in both strains of mice and at each time point, as expected (Fig. 23a, top panel; Fig. 24, 3rd panel from top). Similar results were obtained with cIAP1 expression in that basal levels were lower in cIAP2$^{-/-}$ GAS than in C57BL/6, at both 7 (Fig. 23a, 4th

panel from top) and 14 days (Fig 24, top panel) following denervation, while induction of cIAP1 occurred to the same extent in DEN samples from each mouse.

The E3 ligase known as MuRF1 is well-established to be a highly inducible muscle-specific gene, activated in response to atrophy (Bodine et al., 2001; Gomes et al., 2001; Glass, 2005) and plays a key role in both the development and progression of muscle wasting. As a result, MuRF1 has been validated as a reliable marker of atrophy. In order to determine whether MuRF1 expression levels vary between DEN tissue of cIAP2$^{-/-}$ and C57BL/6 mice, GAS lysates were probed with MuRF1 antibody (see Table 1). As anticipated, wild-type tissue displayed a clear induction following denervation at both 7 (Fig. 23a, 2nd panel from top) and 14 days (Fig. 24, 4th panel from top). cIAP2$^{-/-}$ lysates, however, did not undergo as dramatic an induction of MuRF1 at 7 days post-denervation (Fig. 23a, 2nd panel from top), and even more strikingly less of an induction at day 14 (Fig. 24, 4th panel from top). These results indicate that in the absence of cIAP2, MuRF1 fails to upregulate after denervation to the extent as that seen in C57BL/6 mice, a finding that is consistent with a less atrophic phenotype.

Another marker of atrophy that I chose to investigate was the transcription factor, myogenic differentiation 1 (MyoD). MyoD is a myogenic regulatory factor and has been shown to be sensitive to both increased and reduced mechanical load and to the absence or presence of electrical stimulus (Russo et al., 2010; Legerlotz and Smith, 2008). Various studies have indicated that MyoD levels are affected by denervation atrophy (Eftimie et al., 1991; Hyatt et al., 2003; Ishido et al., 2004; Russo et al., 2007; Russo et al., 2010; Wu et al., 2002) and so I asked whether there would be a difference in MyoD protein expression between cIAP2$^{-/-}$ and C57BL/6 after denervation. To answer this

question, GAS muscle lysates were probed with MyoD antibody (listed in Table 1). The results demonstrated that MyoD protein expression was degraded 7 days following denervation (Fig. 23a, 5th panel from top), and more substantially at 14 days (Fig 24, 5th panel from top) in C57BL/6 gastrocnemius. cIAP2$^{-/-}$ GAS muscle, however, did not show the same decrease in MyoD at day 7 (Fig. 23a, 5th panel from top) and even less at day 14 (Fig. 24, 5th panel from top). These results were in accordance with those seen by Wu and colleagues (2002), who found a decrease in MyoD expression as a result of denervation.

Lastly, I looked at the activity of the alternative (non-canonical) NF-κB pathway in both cIAP2$^{-/-}$ and C57BL/6 hindlimb muscle before and after denervation through western blotting. As previously mentioned, constitutive activation of NF-κB is implicated in both chronic disease state muscle atrophy and disuse conditions (Li et al., 2008). The activity of the alternative NF-κB pathway can be detected by examining the processing of p100 into its mature subunit, p52, which is a crucial activation step. An increase in p100 expression and processing of p52 in both C57BL/6 and cIAP2$^{-/-}$ GAS was consistently observed 7 days following denervation (Fig. 23b). As well, the levels of p100 and p52 were still maintained 14 days after denervation (Fig. 24). Taken together, these results suggest that alternative NF-κB activity is indistinguishable in cIAP2$^{-/-}$ skeletal and wild-type muscle, as a consequence of denervation.

A.

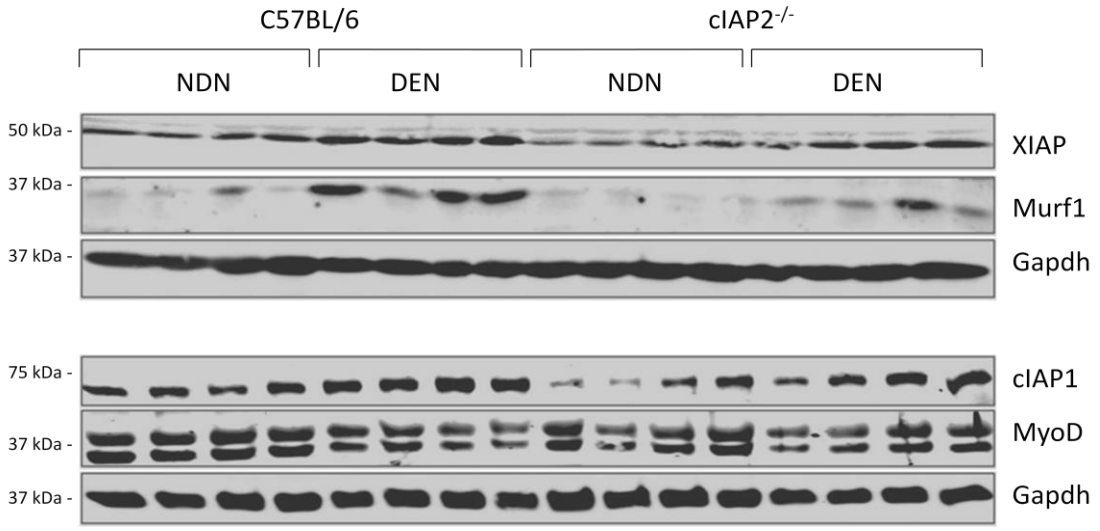

B.

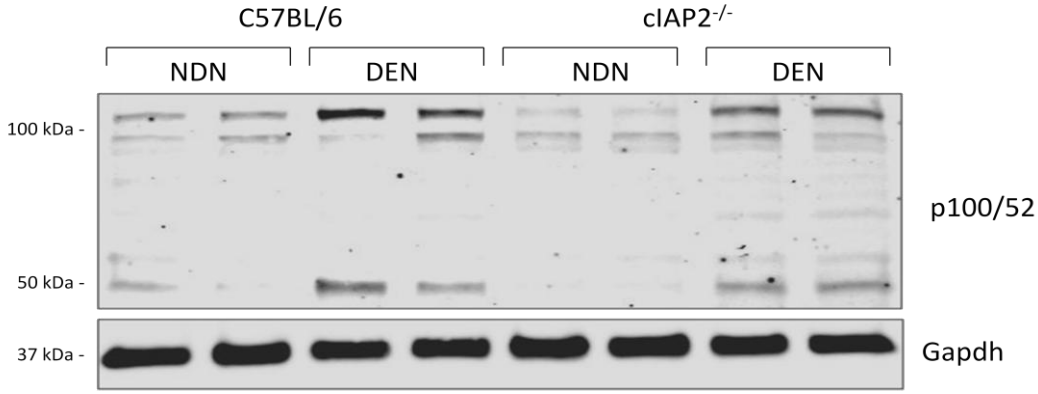

Figure 23. Representative western blots of GAS muscle 7 days following denervation.

Tissue lysates from GAS muscle collected from both C57BL/6 and cIAP2$^{-/-}$ mice 7 days post-denervation were used to immunoblot for various markers of atrophy. XIAP, MuRF1, cIAP1, and MyoD (A) as well as p100/52 (B) protein levels were investigated using their respective antibodies through western blot analysis. Gapdh was used as loading control in both (A) and (B).

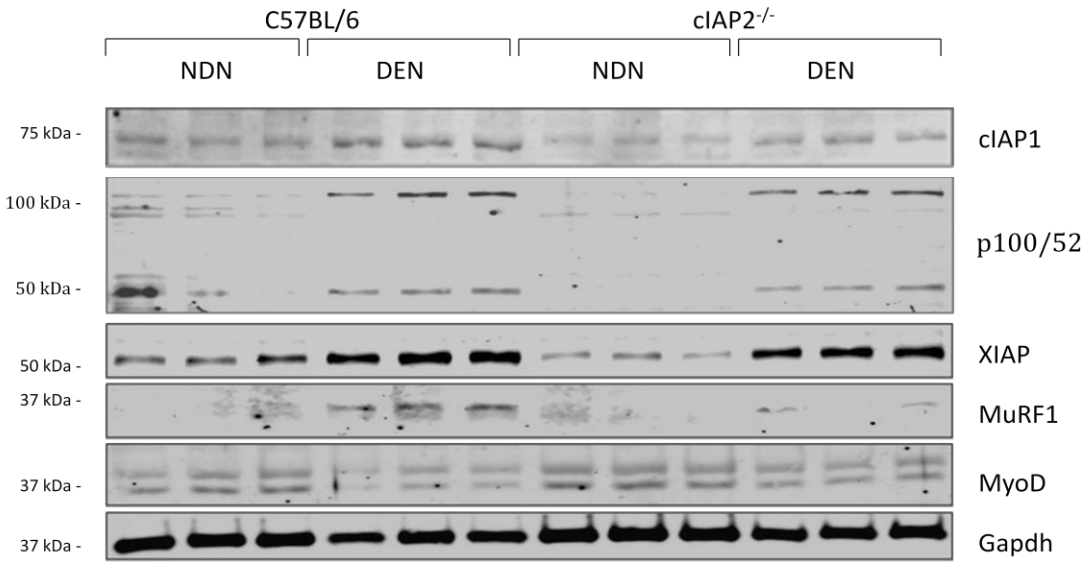

Figure 24. Representative western blots of GAS muscle 14 days following denervation.

Tissue lysates from GAS muscle collected from both C57BL/6 and cIAP2$^{-/-}$ mice 14 days post-denervation were used to immunoblot for various markers of atrophy. cIAP1, p100/52, XIAP, MuRF1, and MyoD protein levels were investigated using their respective antibodies through western blot analysis. Gapdh was used as loading control.

3.1.5 Absence of cIAP2 Protects Soleus Muscle Fibres from Shifting to a Fast Phenotype 14 days After Denervation

My data thus far demonstrate that there is a clear and evident protection against denervation-induced atrophy conferred the absence of cIAP2. A shift in fibre type is expected to occur with atrophy (Lynch et al., 2007; Bigard et al., 1998; Stevenson et al., 2003), from type I fibres to type II. To determine whether there is a failure of fibre type switch and thus, a lack of increase in the number of type II fibres in the absence of cIAP2, immunohistochemical staining was performed on SOL muscle collected after 14 days of disuse (Fig. 25). My results indicate a subtle shift in the percentage of type II fibres in C57BL/6 SOL, which was revealed by a 4% increase in the total number of type II fibres after denervation (Fig. 26). cIAP2$^{-/-}$ SOL, however, only displayed a 0.2% increase in type II fibres (Fig. 26), indicating an insignificant shift following denervation. These results suggest that there is a lack of fibre-type shift in response to denervation in the absence of cIAP2, which further supports the protective phenotype observed against skeletal muscle atrophy in cIAP2$^{-/-}$ mice.

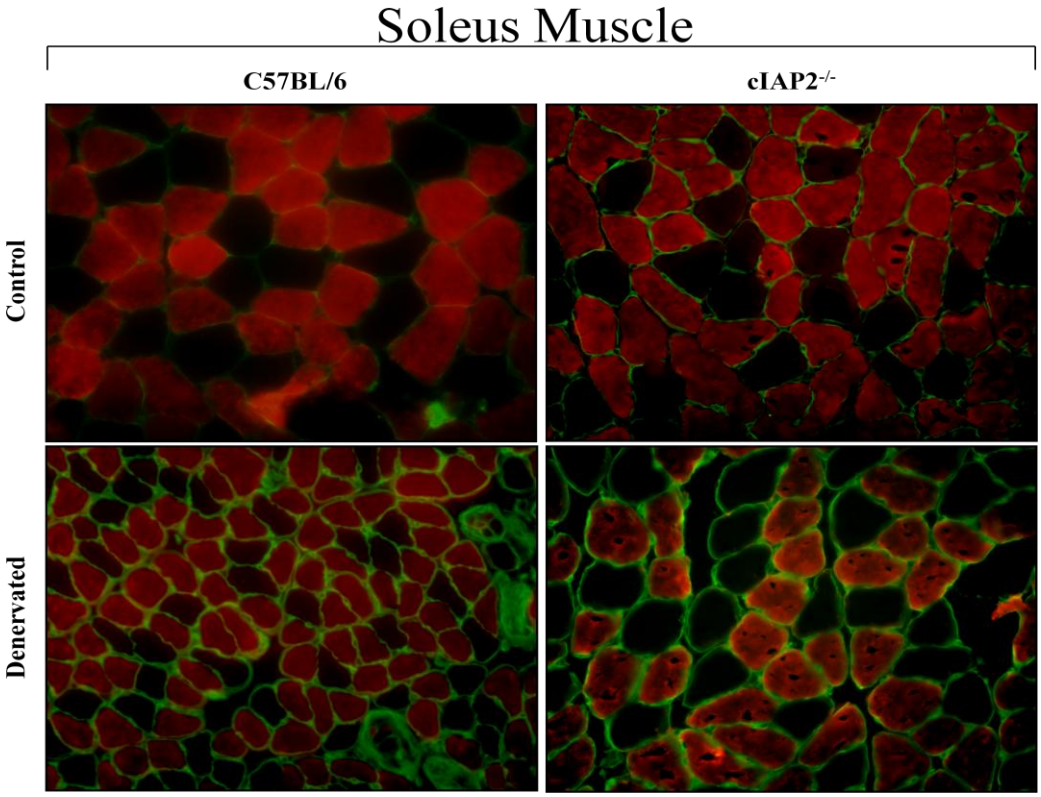

Figure 25. Loss of cIAP2 results in the failure of soleus muscle to undergo the characteristic increase in fast-twitch fibres following denervation.

cIAP2$^{-/-}$ and C57BL/6 mice were denervated as described previously. Ten micrometer cross-sections were made of the soleus muscle 14 days following denervation using a cryostat microtome and immunostained anti-MyHC fast-type and anti-laminin. Images were taken using an Axioskop microscope and Northern Eclipse software. Data was analyzed using Image J software.

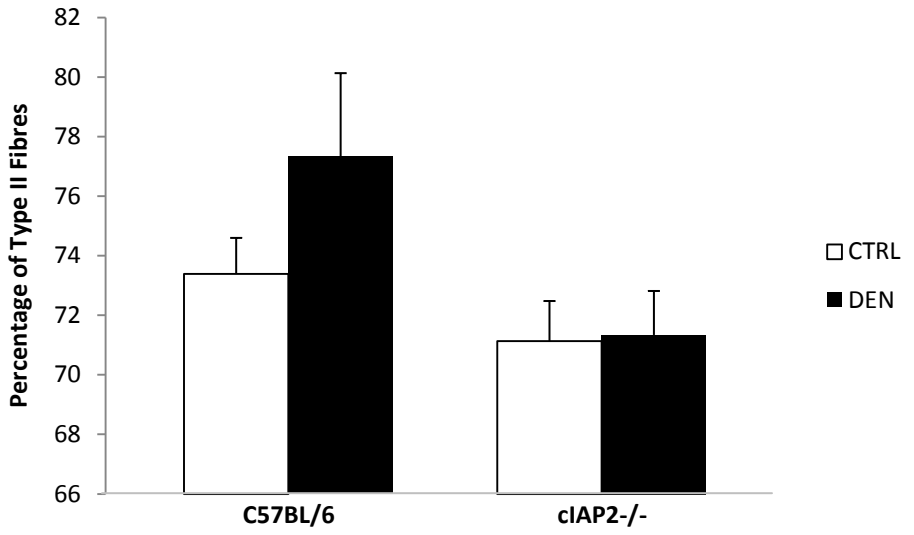

Figure 26. Type I fibres are spared in cIAP2$^{-/-}$ SOL 14 days after denervation.

MHC type I fibres (empty fibres in Fig. 24) and type II fibres (fibres labelled with red in Fig. 24) were counted in SOL muscle cross-sections collected 14 days after denervation using Image J software. I calculated the average percentage of type I fibres in both control and denervated limbs of C57BL/6 and cIAP2$^{-/-}$ mice. n=3 for both cIAP2$^{-/-}$ and C57BL/6 groups. Values represent mean +/- standard error.

3.1.6 Verification of Protective Phenotype in cIAP2$^{-/-}$ Mice Compared to Wild-Type and Heterozygous Littermates

In order to verify that the protection against atrophy seen in cIAP2$^{-/-}$ mice compared to C57BL/6 was not due to strain differences, cIAP2$^{-/-}$ mice were back-crossed with C57BL/6 for four generations to produce both wild-type (WT) and heterozygous (HET) littermate populations. Four-six week old cIAP2$^{-/-}$, WT and HET mice were denervated and the TA muscle was excised 14 days after denervation. TA fibre CSA was measured using H&E stained cross-sections and the average CSA was calculated for both CTRL and DEN limbs of each strain of mouse. Surprisingly, WT and HET TA fibre CSA decreased following denervation by nearly the same amount of 53% and 51% respectively (Fig. 27). In contrast, the fibre CSA was considerably preserved in cIAP2$^{-/-}$ mice after denervation, only decreasing by 35% (Fig. 27). These results are important for three reasons. First, they demonstrate the likelihood that HET littermate populations could be used as functional replacements for WT littermates in future experiments. Second, these data also confirm that cIAP2$^{-/-}$ skeletal muscle is significantly protected against denervation-induced atrophy when compared to WT and HET littermates. Third, these findings demonstrate that the results observed previously in the comparison of cIAP2$^{-/-}$ mice to C57BL/6 did not occur due to strain differences.

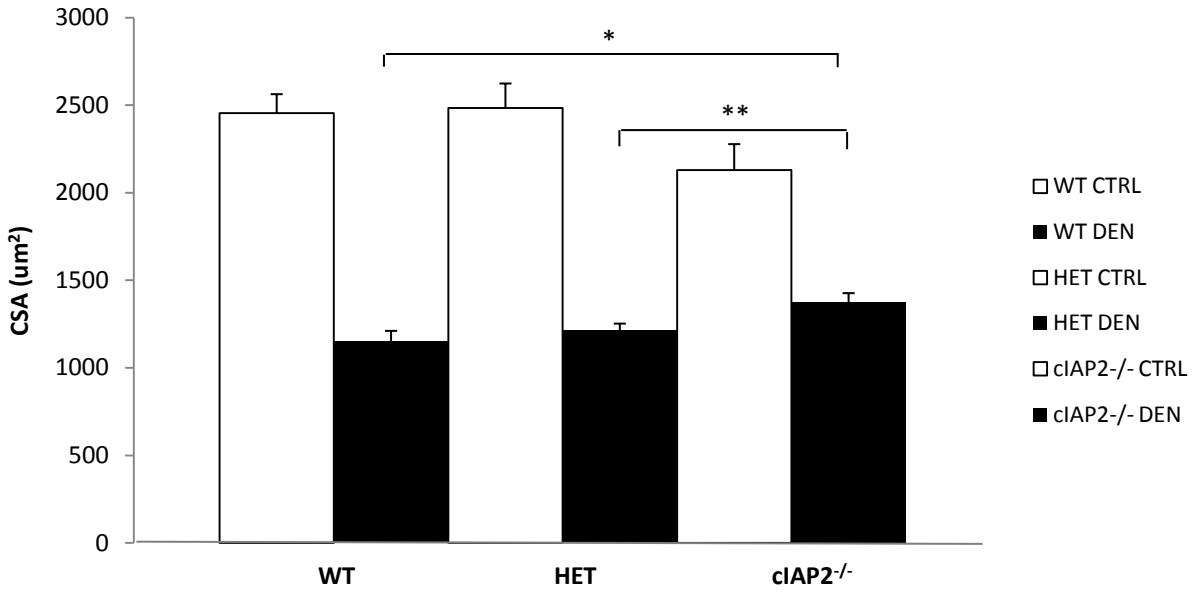

Figure 27. Fibre cross-sectional area is spared 14 days following denervation in cIAP2$^{-/-}$ TA compared to WT and HET littermates.

Fibre cross-sectional area was measured using haematoxylin and eosin stained sections of TA muscle collected from mice 14 days post denervation using Northern Eclipse and Image J software. I measured the average cross-sectional area of both control and denervated limbs in cIAP2$^{-/-}$, WT littermate and HET littermate TA muscles. n=3 for both cIAP2$^{-/-}$ and WT groups; n=4 for HET group. Values represent mean +/- standard error.

3.1.7 Fn14 is not Induced in Response to Denervation

I next asked what possible mechanisms could be responsible for the protection seen against muscle atrophy in the absence of cIAP2. TWEAK is an established potent muscle wasting cytokine (Dogra et al., 2007) and its receptor, Fn14, has been found to be upregulated in response to denervation (Mittal et al., 2010). Taken together, these findings led me to investigate the TWEAK/Fn14 system and its potential mechanistic role in the cIAP2$^{-/-}$ denervation model. I extracted RNA from GAS muscle collected 7 days following denervation from each C57BL/6 and cIAP2$^{-/-}$ mice and Fn14 mRNA levels were measured by quantitative real-time PCR (qRT-PCR) technique (Fig. 28). Remarkably, Fn14 mRNA levels did not change in cIAP2$^{-/-}$ GAS after denervation, while levels increased nearly 5-fold in C57BL/6 (Fig. 28). These results further support the implication that genetically ablating cIAP2 represents a promising approach in preventing the muscle wasting brought forth from denervation. These findings also suggest a potential mechanistic role for the TWEAK/Fn14 system in the protection against denervation-induced atrophy observed in cIAP2$^{-/-}$ mice.

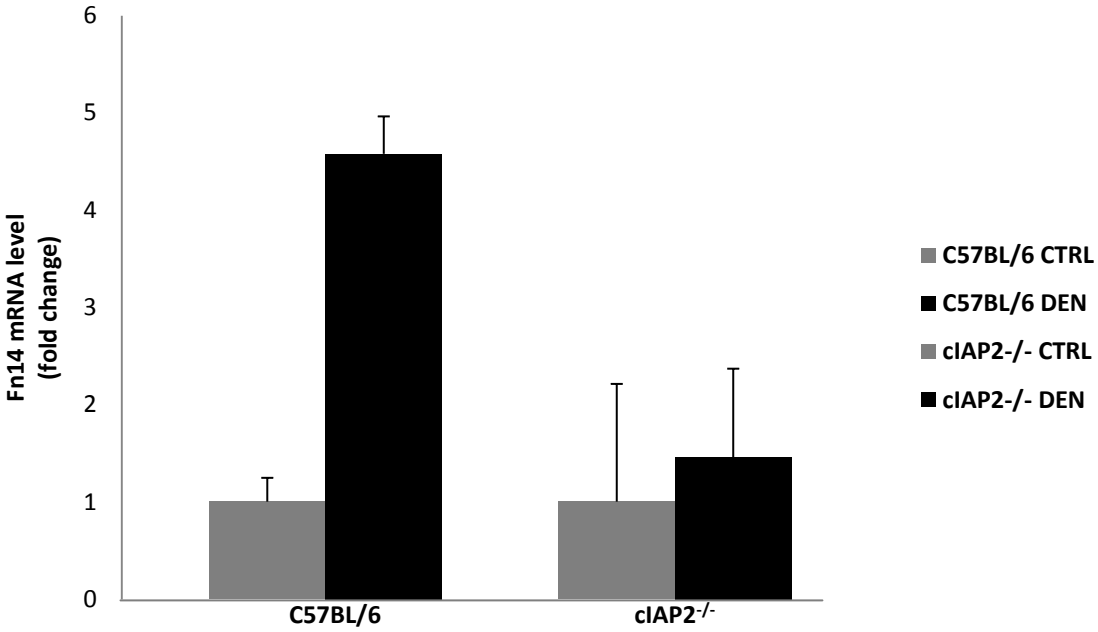

Figure 28. Fn14 induction is inhibited in cIAP2$^{-/-}$ gastrocnemius muscle 7 days following denervation.

qRT-PCR was performed with RNA extracted from homogenized GAS muscle tissue of both C57BL/6 and cIAP1$^{-/-}$ mice, collected 7 days following denervation. mRNA levels of Fn14 were measured in both control and denervated GAS muscles of each genotype. n=2 for C57BL/6 group; n=4 for cIAP2$^{-/-}$ group. Error bars represent standard error.

3.1.8 TWEAK Serum Levels are Unaltered in cIAP2$^{-/-}$ Mice

After demonstrating the difference in Fn14 induction between cIAP2$^{-/-}$ and C57BL/6 mice resulting from denervation, I decided to investigate the levels of TWEAK protein in the serum of each strain of mouse. TWEAK is classified as a key mediator of denervation-induced skeletal muscle atrophy (Mittal et al., 2010), and after determining that Fn14 levels were not upregulated in cIAP2$^{-/-}$ mice, I asked whether TWEAK secretion was affected in the absence of cIAP2. To determine whether TWEAK protein levels varied in cIAP2$^{-/-}$ mice, serum was extracted from mice 7 days following sciatic nerve injury and TWEAK protein levels were measured using an ELISA kit. As shown in Fig. 29, serum levels of TWEAK in cIAP2$^{-/-}$ mice were unchanged compared to those of C57BL/6 mice, suggesting that the genetic ablation of cIAP2 does not cause any change in TWEAK production. This result coupled with the Fn14 qRT-PCR results suggests that cIAP2-loss seems to be affecting targets downstream of TWEAK, disrupting its signalling to Fn14.

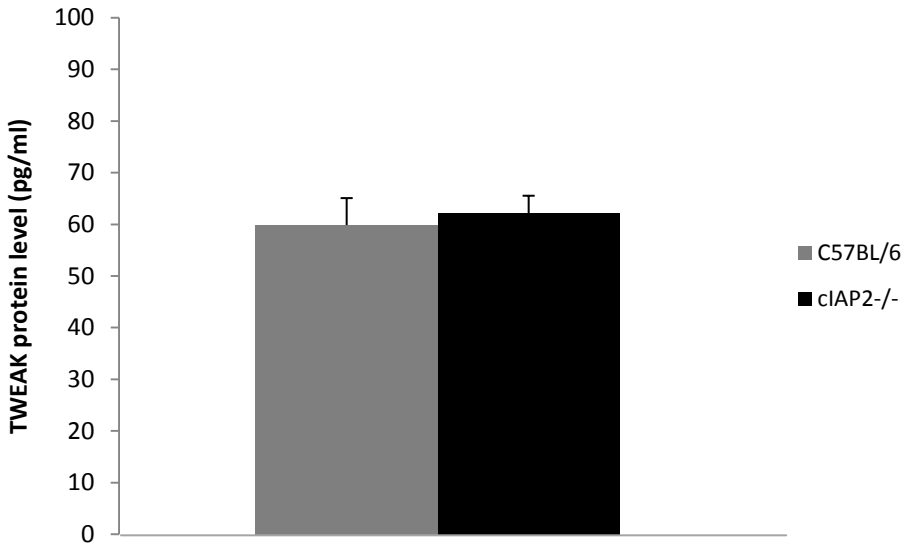

Figure 29. TWEAK serum levels show no significant difference in cIAP2$^{-/-}$ compared to C57BL/6 following hindlimb denervation.

TWEAK ELISA was run on serum collected 7 days post-denervation from both C57BL/6 and cIAP2$^{-/-}$ mice. n=2 for C57BL/6 group; n=4 for cIAP2$^{-/-}$ group. Values represent mean +/- standard error.

3.2 In Vitro Characterization of the Effects of TWEAK on cIAP2$^{-/-}$ Myotubes

3.2.1 cIAP2$^{-/-}$ Myotubes Atrophy in Response to Treatment with Soluble TWEAK

As stated previously, TWEAK has been characterized as a potent muscle wasting cytokine both *in vivo* and *in vitro* (Dogra et al., 2007) and is also implicated to be a mediator of muscle wasting in response to denervation (Mittal et al., 2010). Dogra and colleagues (2007) demonstrated that the addition of soluble TWEAK to cultured C2C12 myotubes rapidly induced muscle wasting and degradation of specific muscle proteins, when compared to control. After determining that Fn14 levels do not increase in response to denervation in cIAP2$^{-/-}$ gastrocnemius muscle, and that TWEAK serum levels were approximately equal in both wild-type and cIAP2$^{-/-}$ mice, I decided to investigate the effects of TWEAK on cultured myotubes lacking cIAP2. The results from this experiment will help to determine whether the observed protection against atrophy is occurring due to either muscle specific or systemic effects. I reasoned that if cIAP2$^{-/-}$ primary myotubes underwent atrophy in response to TWEAK treatment, then the protection against denervation-induced atrophy observed *in vivo*, in the absence of cIAP2, is a result of muscle-extrinsic effects. Wild-type and cIAP2$^{-/-}$ primary myoblasts were grown in 60 mm tissue culture plates and were differentiated into myotubes by incubating in differentiation media for 48 hours. Culture medium was changed and incubated an additional 24 hours with or without the addition of soluble TWEAK (100 ng/ml), and with or without pre-treatment with SMCs (prior to the addition of TWEAK). As expected, wild-type myotubes atrophied in the presence of TWEAK (Fig. 30a), while they maintained their fibre size when pre-treated with SMCs (Fig. 30a). The latter result is consistent with previous results in our laboratory (Mrad et al., unpublished data), and

occurred as a result of cIAP1 degradation by SMCs. Similar to wild-type results, cIAP2$^{-/-}$ myotubes also underwent a large degree of atrophy in response to treatment with TWEAK (Fig. 30b) and were protected when pre-treated with SMCs (Fig. 30b). These results suggest that cIAP2$^{-/-}$ myotubes in culture respond in the same fashion as wild-type myotubes when incubated with soluble TWEAK. This is an indication that the protection against atrophy in the absence of cIAP2 is a result of muscle-extrinsic effects rather than muscle specific effects.

A.

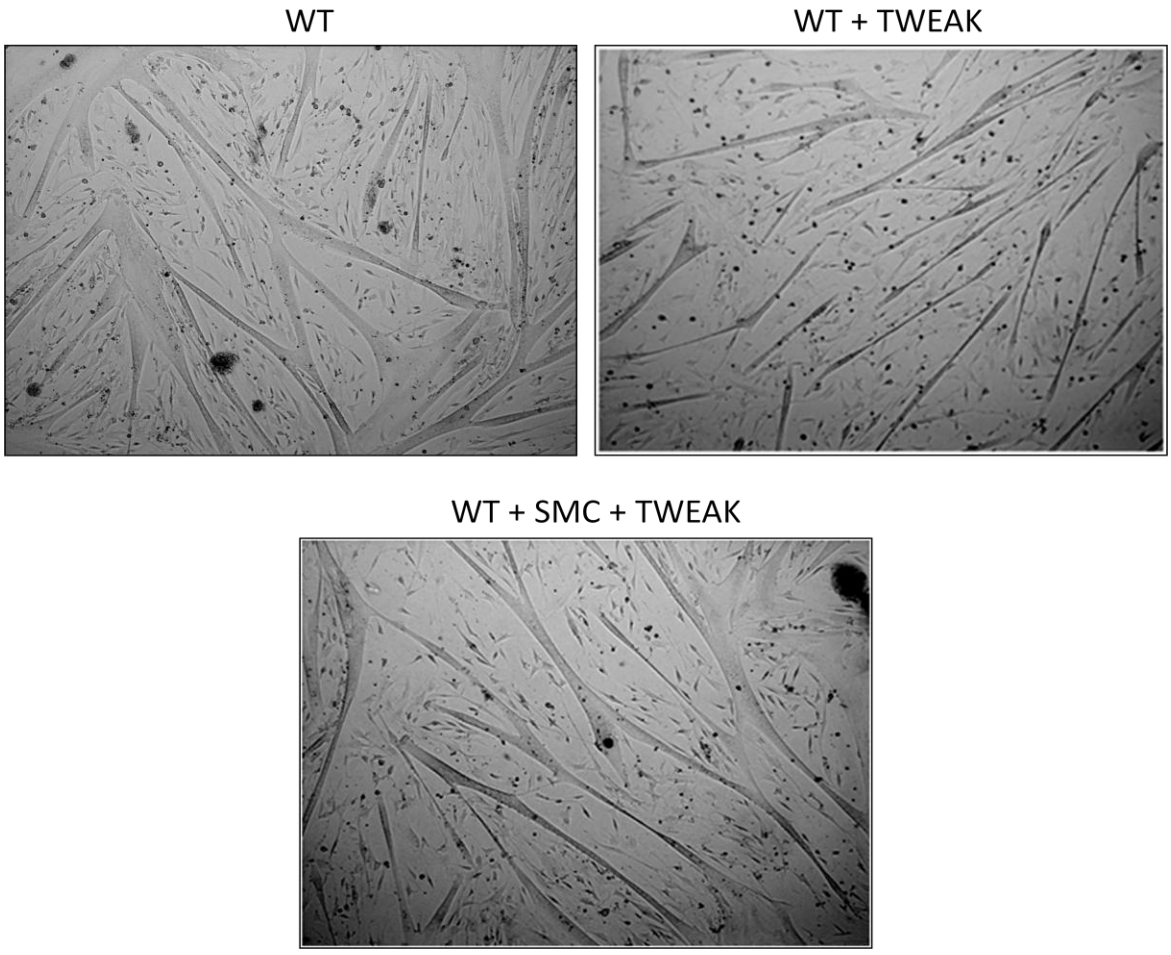

B.

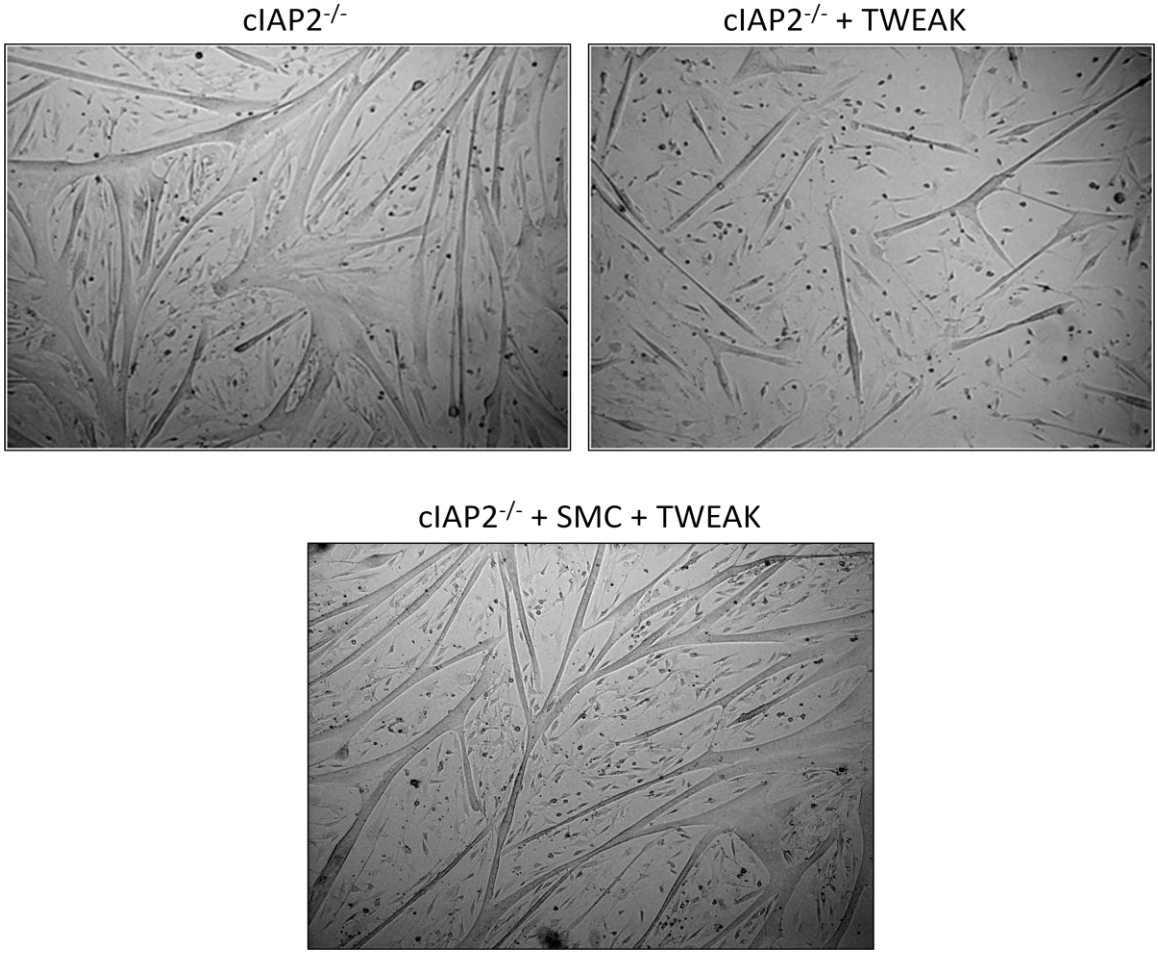

Figure 30. cIAP2$^{-/-}$ primary myotubes respond to TWEAK in a similar fashion as wild-type myotubes.

Wild-type (A) and cIAP2$^{-/-}$ (B) primary myoblasts were differentiated for 2 days (top left panel) and either treated with 100ng/ml of TWEAK alone for 24 hours (top right panel) or pre-treated with 500nm of smac mimetic compound for 0.5 hours prior to treatment with 100ng/ml of TWEAK for 24 hours (bottom panel). Magnification is 20x.

4. Discussion

Skeletal muscle atrophy is a disease state that occurs in response to a number of disuse conditions including denervation, unloading and immobilization (Spate and Schulze, 2004; Glass, 2005; Sandri, 2008). Although the mechanisms behind disuse atrophy are poorly defined, our lab recently established that the loss of cIAP1 protects skeletal muscle against denervation-induced atrophy (Mrad et al., unpublished data). Coinciding with this protection, cIAP2 was also found to be upregulated in muscle tissue as detected by Western blot analyses. I therefore asked whether cIAP2 would play a role in disuse atrophy. The results of my thesis demonstrate, for the first time, a novel role for cIAP2 as a key mediator of denervation-induced skeletal muscle atrophy. Furthermore, Furthermore, the failure of denervation to induce Fn14 in cIAP2$^{-/-}$ muscle suggests that the protection seen in cIAP2$^{-/-}$ mice may result from a blunting of pro-atrophy signalling along the TWEAK/Fn14 axis. Taken together, these results provide sufficient evidence that the modulation of cIAP2 could provide great therapeutic benefit to those burdened with skeletal muscle atrophy.

4.1 Effects of the Loss of cIAP2 on Skeletal Muscle Atrophy

4.1.1 Genetic Ablation of cIAP2 Spares Skeletal Muscle Fibre CSA in Response to Denervation

The data outlined in this thesis were centered primarily around the characterization of the role of cIAP2 in skeletal muscle atrophy. Prior to beginning this work, I had hypothesized that the loss of cIAP2 would result in an increase in the atrophy that occurs as a result of denervation. Remarkably, however, cIAP2-loss resulted in a

marked protection against atrophy. I determined that in the absence of cIAP2, fibre size is spared by ~50% after denervation when compared to controls. In addition, a specific marker of atrophy, MuRF1, was appropriately upregulated in C57BL/6 controls and remained unchanged in cIAP2$^{-/-}$ muscle, further supporting the protective phenotype observed and thus, demonstrating a clear role for cIAP2 in the development and progression of skeletal muscle atrophy.

The triggers initiating disuse atrophy are poorly understood, and so elucidating these mechanisms is an important task in order to fully understand this process of muscle wasting. Previous evidence supports the involvement of the apoptotic pathway in both the initiation and progression of muscle wasting and loss of function (Lynch et al., 2007). A role for the IAPs has not yet, however, been identified in atrophy. The significance of both cIAP1 and cIAP2 in the regulation of TNFα-mediated NF-kB activation was outlined in the introductory chapter. Also outlined, was the importance indicated in the literature of the NF-kB pathway in the loss of skeletal muscle mass involved in muscle atrophy (Li et al., 2008). Based on this knowledge, coupled with our lab's previous findings of cIAP1's role in atrophy (Mrad et al., unpublished data), the potential for cIAP2 participating in the regulation of muscle wasting in some context seemed probable.

While the loss of cIAP2 provides protection from atrophy in several muscle groups, this protection varies from muscle to muscle. Both the TA and SOL muscles displayed the greatest amount of protection against fibre CSA reduction following denervation. The EDL, however, did not display the same level of reduction in atrophy, though protection was still observed. These findings are somewhat confusing in that, the

fibre type composition of the EDL is similar to that of the TA; that is, they each contain predominantly type II (fast-twitch) fibres (Augusto et al., 2004). The SOL, however, is composed primarily of type I (slow twitch) fibres (Augusto et al., 2004). The literature has reported that type I oxidative fibres are more susceptible to disuse atrophy, as the increased inactivity largely affects these fibres due to their frequent and long-standing use during periods of normal activity (Hudson and Franklin, 2002). Type II fibres, on the other hand, are glycolytic and thus used less frequently, at a higher intensity and for shorter periods of time (Symonds et al., 2007). Similar to the individual fibre susceptibility to atrophy, whole muscles composed primarily of slow-twitch fibres are known to atrophy more than fast-twitch muscles and extensors more than flexors (Fitts et al., 2001; Jiang et al., 1992; Ohira et al., 1992; Tischler et al., 1993). Based on this literature, one would hypothesize that muscles containing primarily type II fibres (TA, EDL) would be protected from atrophy on a larger scale than those containing predominantly type I fibres. The level of protection against denervation, however, could likely be directly related to which muscles as a whole are impacted on a greater level by the disuse. If this is the case, then perhaps the explanation as to why the protection in the EDL is diminished in comparison to the TA and SOL muscles, is that the EDL is an extensor muscle, and thus is more susceptible to the effects of disuse. Regardless, the results of this thesis demonstrate a clear and significant protection in cIAP2$^{-/-}$ fibre CSA against denervation-induced atrophy.

4.1.2 Absence of cIAP2 Protects SOL and Fibres from Undergoing the Fibre-Type Switch Characteristic of Atrophy

As briefly described in the introduction, skeletal muscle fibres are classified based on the type of MHC they express. Fibres containing only one form of MHC are known as pure fibres, whereas those containing more than one form of MHC are referred to as hybrid fibres (reviewed in Schiaffino, 2010). Fast-twitch MHC isoforms include type IIa, type IIb and type IId (or IIx), whereas slow MHC is denoted as type I (reviewed in Schiaffino, 2010). During atrophy, a characteristic fibre-type shift occurs in which type I fibres convert into type II fibres (Lynch et al., 2007; Bigard et al., 1998; Stevenson et al., 2003). Fibre-type analysis is often achieved by methods including mATPase histochemistry, immunohistochemistry, and electrophoretic analysis of MHC isoforms contained within a fibre (reviewed in Pette and Staron, 2001). Through immunohistochemical analysis, the results in my thesis do not display a dramatic shift in C57BL/6 SOL after denervation, thus the lack of fibre-type switch that would be expected in cIAP2$^{-/-}$ muscle is not significantly apparent. This, however, could be explained due to the fact that the half-life of MHC has been reported as being approximately two weeks (Tsika et al., 1987). The modifications in MHC expression may therefore not have been detectable within my time point after denervation of 14 days, and so the switch had only just begun at this point. Nonetheless, the small difference that was observed between cIAP2$^{-/-}$ and C57BL/6 SOL would likely increase to a more dramatic difference with a longer period of disuse, as evidence in the literature would suggest (Midrio et al., 1992; Huey and Bodine, 1998; Mourkioti et al., 2006). Investigating fibre-type distribution 28 days after denervation would be an interesting avenue to pursue, as it would likely further support the protective phenotype observed in cIAP2$^{-/-}$ mice against muscle atrophy.

4.1.3 Markers of Atrophy are not Induced in Denervated cIAP2$^{-/-}$ Muscle

Loss of cIAP2 protects muscle from the morphological and physiological indicators of atrophy as previously outlined, and my analyses indicate that the protection applies on a biochemical level as well. The E3 ligase, MuRF1, is normally induced in muscle upon denervation, indicating the initiation of muscle atrophy. A reduced induction of MuRF1 supports a less atrophic phenotype, as indicated in several studies (Mittal et al., 2010; Eddins et al., 2011). Furthermore, the genetic ablation of MuRF1 results in a protection against denervation-induced atrophy (Bodine et al., 2004). In accordance with these studies, the data presented in my thesis demonstrate a significant reduction in the upregulation of MuRF1 after denervation in cIAP2$^{-/-}$ mice. These data support that of the fibre CSA measurements indicating a marked protection against atrophy in the absence of cIAP2.

MuRF1 is contained in the nuclei of muscle cells and is a gene target of NF-κB (Cai et al., 2004). As previously described, the NF-κB pathway is one of the most important pathways involved in skeletal muscle atrophy (Li et al., 2008). In the absence of cIAP2, MuRF1 fails to upregulate compared to control mice, suggesting a disruption in either the activation of NF-κB, or in its ability to signal its target genes. Canonical NF-κB activity would thus be an interesting avenue to explore in this experimental model, as the failure of MuRF1 to upregulate indicates that NF-kB activity could be impaired in the absence of cIAP2.

The process of muscle differentiation is dependent on the activation of a number of various muscle-specific transcription factors, MyoD being one of them (Stewart and Ritwegger, 2006; Pownall et al., 2002). MyoD has also been established to be modulated

in response to both an increase and reduction in mechanical load on the muscle, implicating a potential role for this transcription factor in muscle atrophy. The literature basis for this, however, is somewhat confusing as MyoD levels have been reported to both increase (Eftimie et al., 1991; Hyatt et al., 2003; Ishido et al., 2004; Russo et al., 2007; Russo et al., 2010) and decrease (Wu et al., 2002) in response to denervation. In accordance with Wu and colleagues (2002), my results display a decrease in MyoD levels after denervation in control animals, while these levels are sustained in cIAP2$^{-/-}$ mice. Due to the contradicting results in the literature, however, it is difficult to take away a solid conclusion as to how MyoD is involved in this protection seen against denervation-induced atrophy. With this said, these results displaying sustained MyoD protein levels in cIAP2$^{-/-}$ muscle do serve the purpose of supporting the previous data presented in my thesis.

4.1.4 Involvement of the TWEAK/Fn14 System in the Protection Against Atrophy in the Absence of cIAP2

Although my thesis thus far has clearly demonstrated that mice lacking cIAP2 are significant protected against the atrophy that occurs as a consequence of denervation, the underpinning mechanisms behind this protection are not clear. A number of mechanistic possibilities exist; however, one of the most intriguing possibilities is the potential involvement of the TWEAK/Fn14 system in this protection. Mittal and co-workers (2010) recently demonstrated that the expression of TWEAK's receptor, Fn14, is substantially induced after denervation on both protein and mRNA levels. In accordance with these results, my data indicated a significant induction of Fn14 mRNA in control mice after denervation; yet conversely, Fn14 levels are unchanged in cIAP2$^{-/-}$ muscle.

This result suggests that either TWEAK levels are altered in the absence of cIAP2, or that TWEAK is prevented from activating Fn14 upon denervation. TWEAK serum levels, however, were unaltered in cIAP2$^{-/-}$ mice compared to the control, indicating a disruption in the signalling cascade that leads to Fn14 activation.

cIAP2 has been previously shown to not be expressed in muscle tissue (Mahoney et al., 2008), however the presence of cIAP2 has since been reported by Western blot analysis using muscle tissue (Mrad et al., unpublished datsa). This evidence of cIAP2, nevertheless, is likely from the presence of non-muscle cells, such as fibroblasts, in the lysate. The protection against muscle atrophy observed in the absence of cIAP2 is therefore unlikely to be occurring as a result of an effect intrinsic to muscle. To confirm this, cIAP2$^{-/-}$ primary myoblasts were tested using an *in vitro* correlate of denervation atrophy. The aforementioned results of my thesis indicate that the TWEAK/Fn14 system is potentially involved in the protective phenotype observed in cIAP2$^{-/-}$ mice. As previously described, TWEAK is a potent muscle-wasting cytokine that initiates the degradation of muscle protein through the activation of the ubiquitin-proteasome and NF-κB pathways (Dogra et al., 2007). In contrast to my *in vivo* results, cIAP2$^{-/-}$ myotubes in culture behaved identically to wild-types, thus confirming that the protection in muscle was due to an effect of the loss of cIAP2 systemically. Furthermore, pre-treatment with SMCs was able to prevent both wild-type and cIAP2$^{-/-}$ myotubes from TWEAK-induced atrophy. These results aid in confirming that cIAP2 is likely not expressed in muscle cells, and that any observation of this is likely due to contaminating fibroblasts. Moreover, these data suggest that the protection against muscle wasting in cIAP2$^{-/-}$ mice must be occurring due to systemic effects, rather than muscle-specific effects. Currently,

systemic effects remain unstudied in the context of denervation atrophy, and so further investigation into the mechanisms behind a phenomenon such as this will help to further improve our understanding of skeletal muscle atrophy.

4.1.5 Conclusions and Future Directions

In conclusion, the loss of cIAP2 results in a significant protection against denervation-induced skeletal muscle atrophy. Although the mechanisms behind this protection are unknown, my thesis does provide evidence for the potential involvement of the TWEAK/Fn14 system. Future directions should be aimed toward further characterizing the roles of the TWEAK/Fn14 and NF-κB pathways in the protection against atrophy that occurs in mice lacking cIAP2. While NF-κB is an established target of denervation (Li et al., 2008), it isn't known whether the activation of this pathway is occurring intrinsically or extrinsically to the muscle. The results of my thesis demonstrate a clear induction of Fn14 mRNA in control mice, while levels are unaltered in the absence of cIAP2. As well, I established that TWEAK serum levels were comparable between the two strains of mice, therefore indicating that TWEAK is likely not the cytokine responsible for inducing Fn14 in this model. Evidence in the literature suggests that TWEAK and Fn14 may actually function independently from one another (Tanabe et al., 2003; Polek et al., 2003; Bover et al., 2007), therefore supporting the aforementioned hypothesis. The question thus remains as to what extrinsic factor is responsible for the upregulation of Fn14 after denervation. A likely possibility is that sciatic nerve denervation may lead to the induction of a cytokine other than TWEAK. This particular cytokine could be responsible for activating a component of the NF-κB pathway whose

activity is dependent on the presence of cIAP2. If this is the case, then the lack of Fn14 induction in the absence of cIAP2 could possibly be explained by the impairment of NF-κB signalling, as studies indicate the necessity of the NF-κB pathway in facilitating Fn14 induction (Tran et al., 2006). Although the literature suggests that cIAP1 and cIAP2 play redundant roles in TNFα-mediated NF-κB signalling (Mahoney et al., 2008), this would suggest the potential for individual mediating roles of these two proteins in NF-κB activity. A logical approach in determining whether denervation is in fact inducing a cytokine responsible for targeting NF-kB and in turn, Fn14, would be to investigate the levels of various cytokines that are known to activate NF-κB, by qPCR analysis two days after denervation. Further investigation into both the NF-κB and TWEAK/Fn14 pathways may lead to the mechanism of action behind the absence cIAP2 and protection against muscle atrophy.

In addition to mechanistic studies, investigating the role of cIAP2 in various models of atrophy (i.e., cachexia, casting) would be of interest, to verify whether the loss of this gene protects against a broad spectrum of atrophies. Therapeutically, it would be of great benefit to uncover a role for cIAP2 in other forms of atrophy as well, and I believe, based on my data, that this is a likely possibility. Regardless of the responsible mechanism and further potential implications, however, my data indicate a novel role for cIAP2 in denervation-induced skeletal muscle atrophy. Pharmacological inhibition of cIAP2, therefore, could be used as an approach to treat a number of conditions in which the loss of neural stimulation leads to atrophy and thus, disease progression.

REFERENCES

Goldberg AL. Protein turnover in skeletal muscle. II. Effects of denervation and cortisone on protein catabolism in skeletal muscle. *J Biol Chem*, 1969. 244: 3223-3229.

Alenzi FQ, Lofty M, Wyse RKH. Swords of cell death: Caspase activation and regulation. *Asian Pac J Cancer Prev*, 2010. 11: 271-280.

Ankarcrona M, Dypbukt JM, Bonfoco E, et al. Glutamate-induced neuronal daeth: a succession of necrosis or apoptosis depending on mitochondrial function. *Neuron*, 1995. 15: 961-973.

Attaix D, Ventadour S, Codran A, Bechet D, Taillandier D, Combaret L. The ubiquitin-proteasome system and skeletal muscle wasting. *Essays Biochem*, 2005. 41: 173-186.

Augusto V, Padovani CR, Campos GER. Skeletal Muscle Fiber Types in C57BL6J Mice. *Braz J Morphol Sci*, 2004. 21: 89-94.

Bartoli M, Richard I. Calpains in muscle wasting. *Int J Physiol*, 2005. 37: 2115-2133.

Bigard AX, Boehm E, Veksler V, Mateo P, Anflous K, Ventura-Clapier R. Muscle unloading induces slow to fast transitions in myofibrillar but not mitochondrial properties. Relevance to skeletal muscle abnormalities in heart failure. *J Physiol*, 1998. 548: 649-661.

Bodine SC, Latres E, Baumhueter S, Lai VK, Nunez L, Clarke BA et al. Identification of ubiquitin ligases required for skeletal muscle atrophy. *Science*, 2001. 294: 1704-1708.

Bonfoco E, Krainc D, Ankarcrona M, Nicotera P, Lipton SA. Apoptosis and necrosis: two distinct events induced, respectively, by mild and intense insults with N-methyl-D-aspartate or nitric oxide/superoxide in cortical cell cultures. *Proc Natl Acad Sci USA*, 1995. 92: 7162-7166.

Bover LC, Cardo-Villa M, Kuniyasu A, Sun J, Rangel R, Takeya M, Aggarwal BB, Arap W, Pasqualini R. A previously unrecognized protein-protein interaction between TWEAK and CD163: potential biological implications. *J Immunol,* 2007. 178: 8183-8194.

Burkly LC, Dohi T. The TWEAK/Fn14 pathway in tissue remodeling: for better or for worse. *Adv Exp Med Biol*, 2011. 691: 305-322.

Busquets S, Garcia-Martinez C, Olivan M, Barreiro E, Lopez-Soriano FJ, Argiles JM. Overexpression of UCP3 in both murine and human myotubes is linked with the

activation of proteolytic systems: a role in muscle wasting? *Biochem Biophys Acta*, 2006. 1760: 253-358.

Cai D, Frantz JD, Tawa NE Jr., Melendez PA, Oh BC, Lidov HG, Hasselgren PO, Frontera WR, Lee J, Glass DJ, Shoelson SE. IKKbeta/NF-kappaB activation causes severe muscle wasting in mice. *Cell*, 2004. 119: 285-298.

Cao PR, Kim HJ, Lecker SH. Ubiquitin-protein ligases in muscle wasting. *Int J Biochem Cell Biol*, 2005. 37: 2088-2097.

Centner T, Yano K, Kimura E, McElhinny AS, Pelin K, Witt CC, et al. Idenfication of muscle specific ring finger proteins as potential regulators of the titin kinase domain. *J Mol Biol*, 2001. 306: 717-726.

Charge SBP, Rudnicki MA. Cellular and molecular regulation of muscle regeneration. *Physiol Rev*, 2004. 84: 209-238.

Chicheportiche Y, Bourdon PR, Xu H, Hsu YM, Scott H, Hession C, Garcia I, Browning JL. TWEAK, a new secreted ligand in the tumor necrosis factor family that weakly induces apoptosis. *J Biol Chem*, 1997. 272: 32401-32410.

Conte D, Holcik M, Lefebvre CA, Lacasse E, Picketts DJ, Wright KE, Korneluk RG. Inhibitor of apoptosis protein cIAP2 is essential for lipopolysaccharide-induced macrophage survival. *Mol Cell Biol*, 2006. 26: 699-708.

Costelli P, Reffo P, Penna F, Autelli R, Bonelli G, Baccino FM. Ca2+ -dependent proteolysis in muscle wasting. *In J Biochem Cell Biol*, 2005. 37: 2134-2146.

Goldspink DF. The effects of denervation on protein turnover of rat skeletal muscle. *Biochem J*, 1976. 156: 71-80.

Glass DJ. Molecular mechanisms modulating muscle mass. *Trends Mol Med*, 2003. 9: 344-350.

Glass DJ. Skeletal muscle hypertrophy and atrophy signaling pathways. *Int J Biochem Cell Biol*, 2005. 37: 1974-1984.

Dogra C, Changotra H, Mohan S, Kumar A. Tumor necrosis factor-like weak inducer of apoptosis inhibits skeletal myogenesis through sustained activation of nuclear-facto-kappaB and degradation of MyoD protein. *J Biol Chem*, 2006. 281: 10327-10336.

Eckelman BP, Salvesen GS. The human anti-apoptotic proteins cIAP1 and cIAP2 bind but do not inhibit caspases. *J Biol Chem*, 2006. 281: 3254-3260.

Eddins MJ, Marblestone JG, Kumar KGS, Leach CA, Sterner DE, Mattern MR, Nicholson B. Targeting the ubiquitin E3 ligase MuRF1 to inhibit muscle atrophy. *Cell Biochem Biophys*, 2011. 60: 113-118.

Eftimie R, Brenner HR, Buonanno A. Myogenin and MyoD join a family of skeletal muscle genes regulated by electrical activity. *Proc Natl Acad Sci USA*, 1991. 88: 1349-1353.

Fadeel B, Orrenius S. Apoptosis: a basic biological phenomenon with wide-ranging implications in human disease. *J Intern Med*, 2005. 258: 479-517.

Farges MC, Balcerzak D, Fisher BD, Attaix D, Bechet D, Ferrara M, et al. Increased muscle proteolysis after local trauma mainly reflects macrophage-associated lysosomal proteolysis. *Am J Physiol Endocrinol Metab*, 2002. 282: E326-E335.

Favier FB, Benoit H, Freyssenet D. Cellular and molecular events controlling skeletal muscle mass in response to altered use. *Pflugers Arch - Eur J Physiol*, 2008. 456: 587-600.

Fitts RH, Riley DR, Widrick JJ. Functional and structural adaptations of skeletal muscle to microgravity. *J Exp Biol*, 2001. 204: 3201-3208.

Foletta VC, White LJ, Larsen AE, Leger B, Russell AP. The role and regulation of MAFbx/atrogin-1 and MuRF1 in skeletal muscle atrophy. *Eur J Physiol*, 2011. 461: 325-335.

Furuno K, Goodman MN, Goldberg AL. Role of different proteolytic systems in the degradation of muscle proteins during denervation atrophy. *J Biol Chem*, 1990. 265: 8550-8557.

Glickman MH, Ciechanover A. The ubiquitin-proteasome proteolytic pathway: Destruction for the sake of construction. *Physiol Rev*, 2002. 82: 373-428.

Goldberg AL, Goodman HM. Effects of disuse and denervation on amino acid transport by skeletal muscle. *J Biol Chem*, 1969. 216: 1116-1119.

Goldspink DF, Morton AJ, Loughna P, Goldspink G. The effect of hypokinesia and hypodynamia on protein turnover and the growth of four skeletal muscles of the rat. *Pflugers Arch*, 1986. 407: 333-340.

Gomes MD, Lecker SH, Jagoe RT, Navon A, Godlberg AL. Atrogin-1, a muscle-specific F-box protein highly expressed during muscle atrophy. *Proc Natl Acad Sci USA*, 2001. 98: 14440-14445.

Hasselgreen PO, Menconi MJ, Fareed MU, Yang H, Wei W, Evenson A. Novel aspects on the regulation of muscle wasting in sepsis. *Int J Biochem Cell Biol*, 2005. 37: 2156-2168.

Hershko A, Ciechanover A. The ubiquitin system. *Annu Rev Biochem*, 1998. 67: 425-427.

Huey K, Roy R, Baldwin K, Edgerton V. Temporal effects of inactivity on myosin heavy chain gene expression in rat slow muscle. *Muscle Nerve*, 2001. 24: 517-526.

Huey KA, Bodine SC. Changes in myosin mRNA and protein expression in denervated rat soleus and tibialis anterior. *Eur J Biochem*, 1998. 256: 45-50.

Hunter RB, Stevenson E, Koncarevic A, Mitchell-Felton H, Essig DA, Kandarian SC. Activation of an alternative NF-kappaB pathway in skeletal muscle during disuse atrophy. *FASEB J*, 2002. 16: 529-538.

Hyatt JP, Roy RR, Baldwin KM, Edgerton VR. Nerve activity-dependent regulation of skeletal muscle atrophy: role of MyoD and myogenin in satellite cells and myonuclei. *Am J Physiol Cell Physiol*, 2003. 285: 1161-1173.

Ishido M, Kami K, Masuhara M. In vivo expression patterns of MyoD, p21, and Rb proteins in myonuclei and satellite cells of denervated rat skeletal muscle. *Am J Physiol Cell Physiol*, 2004. 287: 484-493.

Jackman RW, Kandarian SC. The molecular basis of skeletal muscle atrophy. *Am J Physiol Cell Physiol*, 2004. 287: 834-843.

Jackson PK, Eldridge AG, Freed E, Furstenthal L, Hsu JY, Kaiser BK, et al. The lore of the RINGs: Substrate recognition and catalysis by ubiquitin ligases. *Trends Cell Biol*, 2000. 10: 429-439.

Jiang B, Ohira Y, Roy R, Nguyen Q, Ei LK, Oganov V, Edgerton V. Adaptation of fibers in fast-twitch muscle of rats to spaceflight and hindlimb suspension. *J Appl Physiol*, 1992. 73: 58-65.

Jones SW, Hill RJ, Krasney PA, O'Conner B, Peirce N, Greenhaff PL. Disuse atrophy and excercise rehabilitation in humans profoundly affects the expression of genes associated with the regulation of skeletal muscle mass. *FASEB J*, 2004. 18: 1025-1027.

Kandarian SC, Jackson RW. Intracellular signaling during skeletal muscle atrophy. *Muscle Nerve*, 2006 33: 155-165.

kerr JF, Wyllie AH, Currie AR. Apoptosis: a basic biological phenomenon with wide-ranging implications in tissue kinetics. *Br J Cancer*, 1972. 26: 239-257.

Lecker SH, Jagoe RT, Gilbert A, Gomes M, Baracos V, Bailey J, et al. Multiple types of skeletal muscle atrophy involve a common program of changes in gene expression. *FASEB J*, 2004. 18: 39-51.

Lecker SH, Solomon V, Mitch WE, Goldberg AL. Muscle protein breakdown and the critical role of the ubiquitin-proteasome pathway in normal and disease states. *J Nutr*, 1999. 129: 227S-237S.

Lecker SH, Solomon V, Price SR, Kwon YT, Mitch WE, Goldberg AL. Ubiquitin conjugation by the N-end rule pathway and mRNAs for its components increase in muscles of diabetic rats. *J Clin Invest*, 1999. 104: 1411-1420.

Lee SW, Dai G, Hu Z, Wang X, Du J, Mitch WE. Regulation of muscle protein degradation: coordinated control of apoptotic and ubiquitin-proteasome systems by phosphatidylinositol 3 kinase. *J Am Soc Nephrol*, 2004. 15: 1537-1545.

Leeuwenburgh C, Gurley CM, Strotman BA, Dupont-Versteegden EE. Age-related differences in apoptosis with disuse atrophy in soleus muscle. *Am J Physiol Regul Integr Comp Physiol*, 2005. 288: R1288-R1296.

Legerlotz K, Smith HK. Role of MyoD in denervated, disused, and exercised muscle. *Muscle Nerve*, 2008. 38: 1087-1100.

Li H, Malhotra S, Kumar A. Nuclear factor-kappa B signaling in skeletal muscle atrophy. *J Mol Med*, 2008. 86: 1113-1126.

Lorick KL, Jensen JP, Fang S, Ong AM, Hatakeyama S, Weissman AM. RING fingers mediate ubiquitin-conjugating enzyme (E2)-dependent ubiquitination. *PNAS*, 1999. 96: 11364-11369.

Loughna P, Goldspink G, Goldspink DF. Effect of inactivity and passive stretch on protein turnover in phasic and postural rat muscles. *J Appl Physiol*, 1986. 61: 173-179.

Lynch GS, Schertzer JD, Ryall JG. Therapeutic approaches for muscle wasting disorders. *Pharmacol Ther*, 2007. 113: 461-487.

M, Midrio. The denervated muscle: facts and hypotheses. A historical review. *Eur J Appl Physiol*, 2006. 98: 1-21.

M, Sandri. Signaling in muscle atrophy and hypertrophy. *Physiology*, 2008. 23: 160-170.

Mahoney DJ, Cheung HH, Mrad RL, Plenchette S, Simard C, Enwere E, Arora V, Mak TW, Lacasse EC, Waring J, Korneluk RG. Both cIAP1 and cIAP2 regulate TNFalpha-mediated NF-kappaB activation. *Proc Natl Acad Sci U S A*, 2008. 105: 11778-11783.

MB, Reid. Response of the ubiquitin-proteasome pathway to changes in muscle activity. *Am J Physiol Regul Integr Comp Physiol*, 1986. 288: R1423-R1431.

Midrio M, Danieli-Betto D, Megighian A, Velussi C, Catani C, Carraro U. Slow-to-fast transformation of denervated soleus muscle of the rat, in the presence of an antifibrillatory drug. *Pflugers Arch*, 1992. 420: 446-450.

Mittal A, Shephali B, Kumar A, Lach-Trifilieff E, Wauters S, Li H, Makonchuk DY, Glass DJ, Kumar A. The TWEAK-Fn14 system is a critical regulator of denervation-induced skeletal muscle atrophy in mice. *JCB*, 2010. 833-849.

MJ, Tisdale. The ubiquitin-proteasome pathway as a therapeutic target for muscle wasting. *J Support Oncol*, 2005. 3: 209-217.

Monici MC, Aguennouz M, Mazzeo A, Messina C, Vita G. Activation of nuclear factor kappaB in inflammatory myopathies and Duchenne muscular dystrophy. *Neurology*, 2003. 60: 993-997.

Mourkioti F, Kratsios P, Luedde T, Song YH, Delafontaine P, Adami R, Parente V, Bottinelli R, Pasparakis M, Rosenthal N. Targeted ablation of IKK2 improves skeletal muscle strength, maintains mass, and promotes regeneration. *J CLin Invest*, 2006. 116: 2945-2954.

Ohira Y, Jiang B, Roy R, Oganov V, Ilyina-Kakueva E, Marini JF, Edgerton VR. Rat soleus muscle fiber responses to 14 days of spaceflight and hindlimb suspension. *J Appl Physiol*, 1992. 73: 51-57.

Pette D, Staron RS. Transitions of muscle fiber phenotypic profiles. *Histochem Cell Biol*, 2001. 115: 359-372.

Polek TC, Talpaz M, Darnay BG, Spivak-Kroizman T. TWEAK mediates signal transduction and differentiation of RAW264.7 cells in the absence of Fn14/TweakR. Evidence for a second TWEAK receptor. *J Biol Chem*, 2003. 278: 32317-32323

Pownall ME, Gustafsson MK, Emerson CP Jr. Myogenic regulatory factors and the specification of muscle progenitors in vertebrate embryos. *Annu Rev Cell Dev Biol*, 2002. 18: 747-783.

Guttman R. Resistance characteristics of rectifier element in single nerve fibers. *Fed Proc*, 1948.

Rock KL, Gramm C, Rothstein L, Clark K, Stein R, Dick L et al. Inhibitors of the proteasome block the degradation of most cell proteins and the generation of peptides presented on MHC class I molecules. *Cell*, 1994. 78: 761-771.

Roy R, Kim J, Grossman E, Bekmezian A, Talmadge R, Zhong H, Edgerton V. Persistence of myosin heavy chain-based fiber types in innervated but silenced rat fast muscle. *Muscle Nerve*, 2000. 23: 735-747.

Roy R, Zhong H, Monti R, Vallance K, Edgerton V. Mechanical properties of the electrically silent adult rat soleus muscle. *Muscle Nerve*, 2002. 26: 404-412.

Russo TL, Peviani SM, Durigan JLQ, Gigo-Benato D, Delfino GB, Salvini TF. Stretching and electrical stimulation reduce the accumulation of MyoD, myostatin and atrogin-1 in denervated rat skeletal muscle. *J Muscle Res Cell Motil*, 2010. 31: 45-57.

Russo TL, Peviani SM, Freria CM, Gigio-Benato D, Geuna S, Salvini TF. Electrical stimulation based on chronaxie reduces atrogin-1 and MyoD gene expressions in denervated rat muscle. *Muscle Nerve*, 2007. 35: 87-97.

Sacheck JM, Hyatt JPK, Raffaello A, Jagoe RT, Roy RR, Edgerton VR, Lecker SH, Goldberg AL. Rapid disuse and denervation atrophy involve transcriptional changes similar to those of muscle wasting during systemic disease. *FASEB J*, 2007. 21: 140-155.

Saini A, Faulkner S, Al-Shanti N, Stewart C. Powerful signals for weak muscles. *Ageing Research Rev*, 2009. 251-267.

Saitoh T, Nakayama N, Nakano H, Yagita H, Yamamoto N, Yamaoka S. TWEAK induces NF-kappaB2 p100 processing and long lasting NF-kappaB activation. *J Biol Chem*, 2003. 278: 36005-36012.

Scheffner M, Nuber U, Huidbregtse JM. Protein ubiquitination involving an E1-E2-E3 enzyme ubiquitin thioester cascade. *Nature*, 1995. 373: 81-83.

Seol JH, Feldman RM, Zachariae W, Shevchenko A, Correll CC, Lyapina S, et al. Cdc53/cullin and the essential Hrt1 RING-H2 subunit of SCF define a ubiquitin ligase module that activates the E2 enzyme Cdc34. *Gene Dev*, 1999. 13: 1614-1626.

Siu PM, Alway SE. Deficiency of the Bax gene attenuates denervation-induced apoptosis. *Apoptosis*, 2006. 11: 967-981.

SJ, Martin. Dealing with CARDs between life and death. *Trends Cell Biol*, 2001. 11: 188-189.

Spate U, Schulze PC. Proinflammatory cytokines and skeletal muscle. *Curr Opin Clin Nutr Metab Care*, 2004. 7: 265-269.

Spencer JA, Eliazer S, Ilaria RL, Richardson JA, Olson EN. Regulation of microtubule dynamics and myogenic differentiation by MURF, a striated muscle RING-finger protein. *J Cell Biol*, 2000. 150: 771-784.

Stein TP, Wade CE. Metabolic consequences of muscle disuse atrophy. *J Nutr*, 2005. 135: 1824S-1828S.

Stevenson EJ, Giresi PG, Koncarevic A, Kandarian SC. Global analysis of gene expression patterns during disuse atrophy in rat skeletal muscle. *J Physiol*, 2003. 551: 33-48.

Stewart CEH, Rittweger J. Adaptive processes in skeletal muscle: molecular regulators and genetic influences. *J Muskoloskelet Neuronal Interact*, 2006. 6: 73-86.

Symonds BL, James RS, Franklin CE. Getting the jump on skeletal muscle disuse atrophy: preservation of contractile performance in aestivating Cyclorana alboguttata (Gunther 1867). *J Exp Biol*, 2007. 210: 825-835.

Taillandier D, Aurousseau E, Meynial-Denis D, Bechet D, Ferrara M, Cottin P, et al. Coordinate activation of lysosomal Ca2+ -activated and ATP-ubuquitin-dependent proteinases in the unweighted rat soleus muscle. *Biochem J*, 1996. 15: 65-72.

Tanabe K, Bonilla I, Winkles JA, Strittmatter SM. Fibroblast growth factor-inducible-14 is induced in axotomized neurons and promotes neurite outgrowth. *J Neurosci*, 2003. 23: 9675-9686.

Thomason DB, Booth FW. Influence of performance on gene expression in skeletal muscle: effects of forced inactivity. *Adv Myochem*, 1989. 2: 79-82.

Tidball JG, Spencer MJ. Expression of a calpastatin transgene slows muscle wasting and obviates changes in myosin isoform expression during murine muscle disuse. *J Physiol*, 2002. 545: 819-828.

Tischler ME, Henriksen EJ, Munoz KA, Stump CS, Woodman CR, Kirby CR. Spaceflight on STS-48 and earth-based unweighting produce similar effects on skeletal muscle of young rats. *J Appl Physiol*, 1993. 74: 2161-2165.

Tsika RW, Herrick RE, Baldwin KM. Time course adaptations in rat skeletal muscle isomyosins during compensatory growth and regression. *Am Physiol Soc*, 1987. 2111-2121.

Y, Shi. Mechanisms of caspase activation and inhibition during apoptosis. *Mol Cell*, 2002. 9: 459-470.